Mathematical Model of Thermoregulation in Honeybee Swarms

by

Jeremy Chiu

B.Sc. (Hons.), Simon Fraser University, 2013

Thesis Submitted in Partial Fulfillment of the
Requirements for the Degree of
Master of Science

in the
Department of Mathematics
Faculty of Science

SIMON FRASER UNIVERSITY
Fall 2015

Approval

Name:	**Jeremy Chiu**
Degree:	**Master of Science (Applied Mathematics)**
Title:	***Mathematical Model of Thermoregulation in Honeybee Swarms***
Examining Committee:	**Chair:** Dr. Ralf Wittenberg Associate Professor

Dr. JF Williams
Senior Supervisor
Associate Professor _____

Dr. John Stockie
Co-Supervisor
Professor _____

Dr. Razvan Fetecau
Internal Examiner
Associate Professor _____

Date Defended: 3 December 2015

Abstract

Honeybees are masters of regulating their temperatures collectively, even in the absence of a hive. A reproductive swarm consisting of a queen and about half a colony's workers will leave their hive to find a new home. Prior to settling on a permanent home, the honeybees form a stationary swarm, where the bees cling onto one another from a roof-type structure, completely exposed to the elements. Because bees are so sensitive to extremes of heat and cold, it is essential that the swarm has ways to control its temperature. We present a mathematical model to study how honeybees thermoregulate by adjusting their movement and metabolic heat output. We introduce a system of coupled partial differential equations and integral equations to describe the swarm temperature, density, and size, along with a corresponding numerical scheme. We then relax the assumption of spherical symmetry and extend the model by studying non-spherical swarms.

Keywords: Math modelling, bio-mathematics, honeybee swarming, computational PDEs

Dedication

To my family, especially Tige, Cindy, Jason, and Joey.

Acknowledgements

My family for their unconditional support, JF for bringing me into the world of mathematical modelling, John for his immeasurable guidance, AG for changing my work ethic for the better, and finally for all the honeybees – hang in there.

Table of Contents

List of Tables

List of Figures

Chapter 1

Introduction

Reproductive swarming serves as the primary means for honeybee colonies to divide [14, 15, 31, 41]. An old queen with about half a hives workers (ranging from 1,000 to 30,000 bees [15]) will leave their hive in search of a new home, leaving behind developing queens in specialized cells. As the virgin queens are born, they either take some of the remaining workers and also swarm (a process known as *afterswarming*), or stay in the hive and kill the remaining queen bees [41]. Prior to settling on a permanent home, the honeybees searching for a new hive will form a *stationary swarm* (which we henceforth call a *swarm*), where the bees will cling onto one another from a roof-type structure (say a tree branch) while scouts seek a new location [15]. Figures 1.1 and 1.2 depict examples of stationary swarms. The bees will stay in this temporary home until the scout bees, typically the cluster's most experienced foragers, settle on a permanent home [27].

During this period, the swarm may be exposed to ambient temperatures lower than 5°C for a few hours to several days. Considering that honeybees become incapable of flight at temperatures lower than 16°C and incapable of movement at temperatures lower than 5°C [14], the swarm must maintain reasonable temperatures to prevent perishing in the cold. Yet, despite these frigid conditions, it has been documented the swarm can regulate the temperatures to suitable levels – some swarms could maintain their core temperature to within 1°C of 35°C (while most swarms could uphold their temperatures from 30°C to 40°C [29]), while also maintaining their exterior temperature 2°C greater than the ambient temperature or 17°C (whichever was larger) [15]. They must perform this thermoregulation without excessive heat loss, since generating heat by consuming their stores of honey is fatal when their supply is depleted. This task is done by forming a thick layer of immobile bees near the mantle, while the internal part of the swarm (which has no brood or honeycomb hives) can be adapted solely for temperature control [29]. The thermoregulation is so effective that, aside from small swarms with fewer than a thousand bees, the interior bees do not need to produce any excess heat to maintain a temperature of 35°C, their optimal

Figure 1.1: Melbourne swarm, retrieved from `https://commons.wikimedia.org/wiki/File:MelbourneSwarm.JPG`. Used under Creative Commons Attribution-Share Alike 3.0 Unported license [1].

temperature for full activity [29]. In fact, their heat-preservation is so efficient that the swarms often need to adapt the core to expel excess heat [15, 29].

This impressive thermoregulation task is done seemingly without a centralized controller, and without any apparent chemical or acoustic communication between the innermost and outermost bees [15]. Contrary to popular belief, a honeybee colony is not directed by its queen bee – the queen's sole purpose is to lay eggs to maintain a colony's workforce and not to direct the workforce [30]. Hence, the thermoregulation is *self-organized*, meaning the whole swarm's temperature is regulated through individual bees making decisions for themselves. Yet from these decisions being made locally by individual bees, global structures emerge throughout the entire swarm [6, 15]. Although swarm thermoregulation and the similar phenomenon of *winter clusters* (where honeybee colonies may be subjected to freezing temperatures but within the confines of their hive) are well documented [11, 14–17, 25, 29, 31, 34, 35, 41, 42], the processes are not well understood.

Several Eulerian mathematical models on these phenomena have arisen where temperature is modelled by the heat equation, while bee density is treated as a continuum and thus modelled with a partial differential equation (PDE). Earlier models, such as Omholt-Lønvik's [24] model and Lemke-Lamprecht's [20] model, assumed the bees knew about non-local information about the swarm by modelling the metabolic heat output of each bee as a function of the bee's location in the swarm, violating self-organization. Myerscough [22] improved these models by allowing bees to make decisions based solely on local information, but rather than predicting densities, the model simply assumed that density is a function of local temperature. A further refinement of Myerscough's model was presented by Watmough-Camazine [40], where rather than specifying density as a function of temperature, the density profile is described by the local movements of bees. Our thermoregulation model is based on Watmough-Camazine's model, and thus their model is extensively dis-

Figure 1.2: Swarm of honey bees attached to a branch, retrieved from `https://commons.wikimedia.org/wiki/File:Swarm_of_Honey_Bees_attached_to_a_branch.JPG`. Used under Creative Commons Attribution-Share Alike 3.0 Unported license [5].

cussed in Chapter 2. Our work aims to recreate Watmough-Camazine's model and improve their numerical scheme.

Many earlier mathematical models on honeybee thermoregulation, including [8, 20, 22, 24, 40], make the assumption of spherical symmetry. This vastly simplifies the mathematics and computation of the problem because it reduces the number of spatial variables from three to one. There are only a few papers describing models without spherical symmetry, such as models by Basak-Rao-Bejan [4] and Ocko-Mahadevan [23]. Moreover, Sumpter-Broomhead [37] present an agent-based model which allows the shape to be non-spherical. These models are discussed in Chapter 4, where we examine how to relax the spherical symmetry assumption.

In this thesis, we present our extension of Watmough-Camazine's model, which we describe in detail in Chapter 2. We then discuss our numerical scheme to simulate our model in Chapter 3, and display the numerical convergence studies along with physical results. Afterwards, in Chapter 4, we discuss a method for relaxing the assumption of spherical symmetry by deriving a model of a swarm in a hemisphere. Finally, in Chapter 5 we discuss possible extensions to our model.

Chapter 2

Thermoregulation Model of Watmough and Camazine

Our work is based on the model presented by Watmough and Camazine in the paper, *Self-Organized Thermoregulation of Honeybee Clusters* [40]. Hence, we go over the key features and results of the model in detail. We refer to the authors and their paper as WC.

2.1 Model Assumptions

The WC model makes 7 key assumptions:

1. The swarm contains a large enough population of bees at high enough densities that it can be approximated as a continuum. Thus quantities such as bee density can be defined and treated as continuous functions.

2. Bees are self-organized and have no centralized controller, with individuals responding only to local conditions.

3. A bee will move in the direction of decreasing temperature when too warm. Similarly, a bee will move in the direction of increasing temperature when too cold.

4. Bees generate heat both passively and actively, especially when cold.

5. The swarm is spherically symmetric.

6. Heat transfer in the swarm interior is through conduction between neighbouring bees.

7. Bees are conserved and hence no bees leave or enter the swarm.

Modelling the swarm as a continuum of bees (Assumption 1) makes the problem continuous rather than discrete. Hence differential equations can be used to describe heat transfer

and bee movement. This assumption is reasonable because bee swarms are observed to be quite packed and dense, at least when the ambient temperature is low [14]. In contrast to a discrete model, the continuum model fails to capture certain small-scale dynamics. For instance, it is observed that cold bees on the surface of the swarm may push their way into the warmer interior, thus exposing new bees to the exterior [14]. In this case when bees are switching places, the continuum model would fail to capture this phenomenon. Despite this, we use a continuum model rather because discrete models are much more computationally expensive, even when simulating small swarms of honeybees.

Self-organization has several meanings in the literature [3, 9]. We use self-organization (Assumption 2) to mean that bees in a swarm do not possess a centralized controller, and thus the structure that emerges in the swarm is the result of individual bees making decisions based on local conditions. This is consistent with the finding that there is no centralized controller directing bees where to move or how to stay warm [32], and with the observation that there is no communication between the swarm centre and exterior [15]. Mathematically, this means that the governing equations describing a fixed location will only depend on local properties of the swarm such as density or temperature.

Assumptions regarding the thermoregulation mechanism (Assumptions 3 and 4) are based on experimental results. Bee movement can only be described qualitatively rather than quantitatively since, to our knowledge, there is no experimental data describing how bees move in response to change in the swarm. On the other hand, their heat production has been measured in experiments (see Section 2.3.2).

Spherical symmetry (Assumption 5) is a mathematically convenient assumption that allows us to study the problem in just one spatial variable (distance from the origin, r) rather than three variables, which greatly simplifies the model and accelerates the computations. This assumption matches observations reasonably well at colder ambient temperatures; however, the spherical symmetry breaks down at warmer ambient temperatures when the swarm is observed to become elongated [15]. Furthermore, other physical effects may break the spherical symmetry including gravity, the structure the swarm clings onto (such as a tree branch), or asymmetry in heat convection. In Chapter 4, we explore the problem of swarm thermoregulation without spherical symmetry.

Assuming heat transfer is dominated by heat conduction (Assumption 6) means that we may ignore the effects of heat convection. This seems reasonable because the swarm is stationary, and because the denseness of the swarm results in little air flow throughout the cluster. However, during warmer ambient temperatures, the swarm is less crowded, and it is observed that ventilating channels emerge within the swarm that allow the interior to rapidly cool [15]. When this occurs, heat convection becomes more important than heat conduction, and thus Assumption 6 no longer holds.

Conservation of bees (Assumption 7) is used to derive an equation for the dependent variable R, the swarm radius. Strictly speaking this assumption is not correct since bees may

die. Bees left on the exterior of the swarm for too long may consume all their honey stores, eventually leading them to become immobile, falling off the swarm, and freezing [15]. This is especially common when bee clusters swarm for prolonged periods of time, or for smaller bee swarms (i.e., less than 6,000 bees) [15]. Nevertheless, this assumption is acceptable so long as the timescale of a simulation is not too long (shorter than three days) so that not too many bees would die. Additionally, scouts seeking a new location for a permanent hive will leave and enter the swarm, relaying information about potential nest sites with other scouts; however the number of scouts is small (roughly 5% [27]), so the change in swarm numbers due to scouts coming and going may also be ignored.

2.2 Mathematical Formulation

In order to study the swarming phenomenon mathematically, we need to define both independent and dependent variables, their governing equations, and their constitutive functions. Furthermore, boundary conditions are imposed to describe how the exterior of the swarm interacts with the ambient air.

2.2.1 Variables

In order to create their model, WC introduce two independent variables, time t and space r. Note that rather than dealing with three spatial dimensions, Assumption 5 reduces the space dependence to the distance from the origin, radius $r \in \mathbb{R}^1$, $r \geq 0$. Since we are interested in how bees move to adapt to cold temperatures, WC also introduce dependent variables temperature $T = T(t, r)$ [°C] and bee density $\rho = \rho(t, r)$ [dg cm^{-3}]. Finally, the size of the swarm is allowed to change in time, so that $R = R(t)$ [cm] is defined as the time-dependent radius of the swarm.

Note that Assumption 1 allows the density to be treated as a continuous variable. We will aim to compare our results with biological experiments which report a *number* of bees rather than a *mass* of bees, and thus would like to eventually describe the density as a number of bees. Heinrich [15] uses 115 mg as a standard weight for a bee, and reports that a European honeybee worker with an empty stomach weights 93 mg. As such, we assume each bee weights $\frac{1}{10}$ g, or 1 dg. Thus we use the convention that $\rho = n$ corresponds to n bees, and hence bee mass can be described by a number of bees.

In addition to these variables, we also require the following constitutive functions:

- $\lambda(\rho)$, the thermal conductivity of bees [W cm^{-1} K^{-1}], describes how heat is passed along the bees based on how crowded they are (Assumption 6);
- $f(T)$, the metabolic heat production of a bee [W dg^{-1}], models the passive and active heat production of bees as a function of local temperature (Assumption 4);

- $\mu(\rho)$, the motility function [cm^2 s^{-1}], a barrier function that has little physical relevance which forces the swarm to be neither too sparse nor too dense;
- and $\chi(T)$, the thermotactic velocity [cm^2 K s^{-1}], outlines whether bees are driven to warm or cold regions (Assumption 3).

The functions are thoroughly explained in Section 2.3, and a summary of all the variables and parameters is presented in Table 2.2.

2.2.2 Equation for Swarm Temperature

WC model the swarm temperature $T(t, r)$ using the heat equation, which has a diffusive term that captures the mechanism of heat conduction (Assumption 6), and a source term encompassing the heat production of bees (Assumption 4). Thus we have

$$c\frac{\partial T}{\partial t} = \nabla \cdot (\lambda(\rho)\nabla T) + \rho f(T), \tag{2.1}$$

where c is the heat capacity of the swarm [J °C cm^{-3}], λ the thermal conductivity, and f a source term that describes the metabolic heat output per bee. In spherical coordinates with symmetry about the origin, this becomes

$$\frac{\partial T}{\partial t} = \frac{1}{r^2}\frac{\partial}{\partial r}\left[r^2\lambda(\rho)\frac{\partial T}{\partial r}\right] + \rho f(T). \tag{2.2}$$

2.2.3 Equation for Bee Density

To capture variations in bee density $\rho(t, r)$ Assumptions 2 and 3 must be accounted for, along with the fact that bees do not want to be overly crowded or spread out. Thus to describe change in density, it is assumed the bees move along the temperature and density gradient levels according to the advection-diffusion equation

$$\frac{\partial \rho}{\partial t} = \nabla \cdot (\mu(\rho)\nabla\rho) - \nabla \cdot (\chi(T)\rho\nabla T), \tag{2.3}$$

where μ is the bee motility and χ is a thermotactic velocity. In spherical coordinates with symmetry about the origin, this becomes

$$\frac{\partial \rho}{\partial t} = \frac{1}{r^2}\frac{\partial}{\partial r}\left[r^2\mu(\rho)\frac{\partial \rho}{\partial r}\right] - \frac{1}{r^2}\frac{\partial}{\partial r}\left[r^2\chi(T)\rho\frac{\partial T}{\partial r}\right]. \tag{2.4}$$

This equation is similar to other mathematical models for chemotaxis; the reader is directed to [21, Chapter 1.3] for an example.

2.2.4 Equation for Swarm Radius

Bee swarms are observed to expand or contract in response to changes in the ambient temperature [15]. As such, the radius of the swarm is allowed to vary with time. We can count the total initial number of bees B_0 by integrating across the initial spherical swarm of radius $R(0)$

$$4\pi \int_0^{R(0)} r^2 \rho(0, r) \mathrm{d}r = B_0.$$

According to Assumption 7 the total number of bees is constant in time, so we obtain

$$4\pi \int_0^{R(t)} r^2 \rho(t, r) \mathrm{d}r = B_0. \tag{2.5}$$

Rather than dealing with two partial differential equations (2.1), (2.3) and one integral equation (2.5), WC transform this integral equation into a differential equation by taking the time derivative of Equation (2.5) to obtain

$$\frac{\mathrm{d}R}{\mathrm{d}t} = \left(-\frac{\mu}{\rho} \frac{\partial \rho}{\partial r} + \chi \frac{\partial T}{\partial r} \right) \Bigg|_{r=R(t)}. \tag{2.6}$$

The derivation of this differential equation is discussed in Appendix A.1.

2.2.5 Boundary Conditions

The spherical swarm geometry requires imposing boundary conditions at the centre of the sphere (a computational boundary) and the exterior of the swarm. We often refer to the exterior as the swarm *mantle* or *surface*.

For the core, from Assumption 5, spherical symmetry gives the boundary conditions

$$\frac{\partial T}{\partial r}(t, 0) = 0, \tag{2.7}$$

$$\frac{\partial \rho}{\partial r}(t, 0) = 0. \tag{2.8}$$

Heat loss at the exterior is assumed to obey Newton's law of cooling

$$\left(\lambda(\rho) \frac{\partial T}{\partial r} \right) \Bigg|_{r=R(t)} = h_c \left(T_a(t) - T(R(t), t) \right), \tag{2.9}$$

where h_c is the average rate of convective heat transfer [W $^\circ\mathrm{C}^{-1}$ cm^{-2}] at the surface and $T_a(t)$ is the ambient temperature [$^\circ$C].

The density on the exterior is taken to satisfy the Dirichlet boundary condition

$$\rho(R(t), t) = \rho_R, \tag{2.10}$$

where ρ_R is some constant representing the number of bees on the outermost layer of the swarm, typically chosen between 2 to 5. WC claim they experimented with boundary conditions dependent on the ambient temperature and cluster radius, neither of which gave significant changes in the results.

WC do not discuss their choice of initial conditions, and so we can only estimate them from the given solution plots.

2.3 Constitutive Functions

In addition to the three key dependent variables (temperature, bee density, and swarm radius), four important constitutive functions are used in the model. Aside from μ, these are all motivated by experimental observations and fit to measured data on actual bees.

2.3.1 Conductivity λ

A bee's heat conductivity is typically less than that of air and depends on how tightly packed the bees are, so the thermal conductivity coefficient is treated as a function of density. Fundamentally, the conductivity of the swarm $\lambda = \lambda(\rho)$ must decrease as density increases. Hence the conductivity of a very dense group of bees is nearly zero, allowing a thick layer of bees to act as an insulating layer. Conductivity λ is modelled by the equation

$$\lambda(\rho) = \lambda_{air} - (\lambda_{air} - \lambda_{bee}) \left(\frac{\rho}{10}\right)^{\frac{2}{3}}, \tag{2.11}$$

where the heat conductivity of λ_{air} is assumed to be greater than that of the typical bee conductivity λ_{bee}. For the computation, $\lambda_{air} = 10$ mW/cm°C and $\lambda_{bee} = \frac{\lambda_{air}}{2}$. Since there is a lack of experimental data regarding the conductivity of a bee swarm, this equation assumes that local conductivity depends solely on local density. This particular choice of λ_{air} and λ_{bee} is in agreement with data reported in [33]. A plot of $\lambda(\rho)$ is given in Figure 2.1.

2.3.2 Metabolic Heat Production f

According to Assumption 4, bees generate heat passively, while also generating heat metabolically when cold. To model this effect, the function $f = f(T)$ is introduced, which describes heat production by individual bees in both warm and cold temperatures. Passive heat production in warm air is assumed to have a Q_{10} coefficient of 2.4 [18, 20], which suggests that

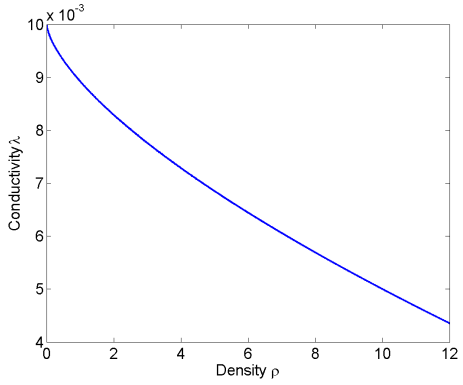

Figure 2.1: Coefficient of heat conductivity as a function of bee density, in W cm^{-1} K^{-1}.

the resting metabolic output increases by a factor of 2.4 for every 10°C increase in local temperature. The reader is directed to [13] for a discussion of the Q_{10} thermal coefficient.

For cold temperatures, when a bee is colder than the shivering temperature T_s, it increases its heat production 50-fold by shivering until T_m, where their heat production caps at the metabolism of a bee in flight (50mW). This gives the following expression

$$f(T) = \begin{cases} 50 f_{18}, & \text{if } T < T_m, \\ 50 f_{18} e^{\alpha(T_m - T)}, & \text{if } T_m \le T < T_s, \\ f_{18}(2.4)^{\frac{T-18}{10}}, & \text{if } T \ge T_s, \end{cases} \tag{2.12}$$

where f_{18} is the resting metabolism of a bee at 18°C and the constant α is chosen so that $f(T)$ is continuous at $T = T_s$. Some arithmetic shows that to ensure continuity, we require

$$\alpha = \frac{\frac{T_s - 18}{10}\log(2.4) - \log(50)}{T_m - T_s}. \tag{2.13}$$

Typically, T_m is assumed to be 15°C, while T_s is about two degrees greater than T_m. Also, f_{18} is taken to be 1 mW/dg. The function $f(T)$ and its parameter values are in reasonable agreement with results from [18, 20, 28, 34]. A plot of $f(T)$ is given in Figure 2.2. The reader is directed to [12] for a further reading on experimental data on the metabolism of individual honeybees.

2.3.3 Motility μ

In order to maintain bee densities at a desirable level, we introduce the motility function $\mu = \mu(\rho)$. When bees are too crowded or spread out, the motility increases exponentially. With such motility, the bees are forced to within a desired density range. This function is artificial and has no direct physical relevance; rather, it serves as a "barrier function" that

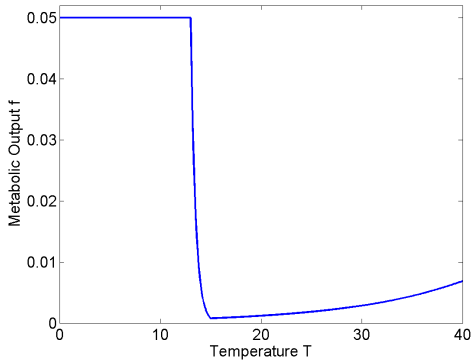

Figure 2.2: Metabolic heat production of a single bee f as a function of local temperature T, in W dg^{-1}.

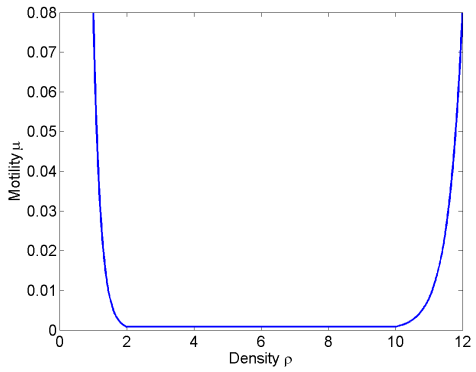

Figure 2.3: Motility μ as a function of density, in cm^2 s^{-1}.

forces the bee density to lie within the domain $[2, 10]$. Such a function is

$$\mu(\rho) = \begin{cases} \mu_0(100)^{2-\rho}, & \text{if } \rho < 2; \\ \mu_0, & \text{if } 2 \leq \rho \leq 10; \\ \mu_0(10)^{\rho-10}, & \text{if } 10 < \rho \leq 13; \\ 1000\mu_0, & \text{if } \rho > 13. \end{cases} \tag{2.14}$$

The motility function $\mu(\rho)$ is plotted in Figure 2.3. Note that the shape of the graph is important, not its absolute scale.

2.3.4 Thermotactic Velocity χ

The thermotactic velocity $\chi = \chi(T)$ describes how bees move in the direction of increasing temperature. Fundamentally, this function is positive if the local temperature is below T_h (the huddling temperature) and negative otherwise. Hence bees move up the temperature gradient when cold and down the temperature gradient when warm. For simplicity, WC

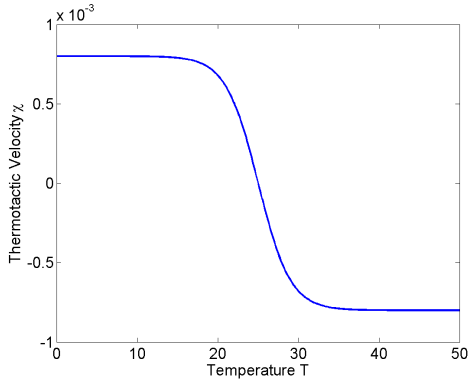

Figure 2.4: Thermotactic velocity χ as a function of local temperature, in cm $^\circ\text{C}^{-1}$ s^{-1}.

use the hyperbolic tangent function

$$\chi(T) = \chi_0 \tanh\left(\frac{T_h - T}{4}\right),$$

which is plotted in Figure 2.4 for values of $\chi_0 = 10^{-3}$ and $T_h = 25$.

2.3.5 Ambient Temperature

To simulate bees responding to the temperature changes over the course of a day, we use a sinusoidal ambient temperature function with mean T_{mean} and amplitude T_{amp}. We typically take the mean temperature as 0°C and the amplitude no greater than 15°C.

2.3.6 Typical Parameter Values

In Table 2.1, we state the default parameter values for numerical simulations. All of these are explicitly stated in [40, Figure 5], except for f_{18}, T_m, T_s, and ρ_R. We found f_{18} from [40, Figure 2], while T_m, T_s, and ρ_R were guessed by inspecting figures throughout [40]. Moreover, in Table 2.2, we present a summary of all our parameters and variables along with some typical values.

Parameter	**Value**
B_0	8,104 dg
T_{amp}	15°C
T_h	25°C
T_m	13°C
T_{mean}	0°C
T_s	15°C
c	1 J °C cm^{-3}
f_{18}	1×10^{-3} W dg^{-1}
h_c	2.5×10^{-3} W $°C^{-1}$ cm^{-2}
h_f*	2×10^{-3} W $°C^{-1}$ cm^{-2}
λ_{air}	10×10^{-3} W $°C^{-1}$ cm^{-1}
λ_{bee}	5×10^{-3} W $°C^{-1}$ cm^{-1}
μ_0	8×10^{-4} cm^2 s^{-1}
ρ_R	2 dg cm^{-3}
χ_0	8×10^{-4} cm $°C^{-1}$ s^{-1}

Table 2.1: The typical parameter values we used in the numerical simulations. * note that h_f is not used in the one-dimensional simulations.

Symbol	Quantity	Units	Typical Values
B_0	Initial number of bees	dg	5,000 to 30,000
M	Number of points in discretization in ϕ (2D)	dimensionless	2^3 to 2^5
N	Number of points in discretization in x or r	dimensionless	2^4 to 2^9
$R(t)$	Radius of swarm	cm	Equation (2.5)
$T(t,r)$	Temperature of swarm at a point	°C	Equation (2.1)
$T_a(t)$	Ambient temperature	°C	$T_{mean} \pm T_{amp}$
T_{amp}	Ambient temperature amplitude	°C	0 to 15 *
T_h	Thermotactic huddling temperature	°C	25 *
T_m	Minimum temperature bees continue to increase shivering	°C	1 to 3 less than T_s †
T_{mean}	Mean ambient temperature	°C	usually 0 *
T_s	Temperature bees begin to shiver	°C	3 to 15 †
c	Heat capacity of honeybees	J °C cm^{-3}	≤ 1 *
$f(T)$	Metabolic heat production of bees	W dg^{-1}	0 to $50 f_{18}$
f_{18}	Resting heat production of bees at 18°C	W dg^{-1}	1 mW per bee †
h_c	Rate of heat convection at swarm surface	W $°C^{-1}$ cm^{-2}	about 2.5×10^{-3} *
h_f	Rate of heat convection at roof (2D)	W $°C^{-1}$ cm^{-2}	2×10^{-3} [7]
r	Distance from cluster centre	cm	0 to $R(t)$
t	Time	s	0 to t_f
t_f	Final time	s	$\leq$ 3 days *
Δt	Time-step	s	10^{-3} to 1, depending on N
$\lambda(\rho)$	Heat conduction coefficient	W $°C^{-1}$ cm^{-1}	0 to λ_{air}
λ_{air}	Heat conductivity of air	W $°C^{-1}$ cm^{-1}	10×10^{-3} *
λ_{bee}	Heat conductivity of a bee	W $°C^{-1}$ cm^{-1}	$\frac{1}{2}\lambda_{air}$ *
$\mu(\rho)$	Motility function	cm^2 s^{-1}	μ_0 to 10,000 μ_0
μ_0	Motility coefficient	cm^2 s^{-1}	8×10^{-4} *
$\rho(t,r)$	Density of bees	dg cm^{-3}	Equation (2.3)
ρ_R	Density of bees at swarm surface	dg cm^{-3}	2 to 5 †
$\chi(T)$	Thermotactic velocity function	cm $°C^{-1}$ s^{-1}	$-\chi_0$ to χ_0
χ_0	Thermotaxis coefficient	cm $°C^{-1}$ s^{-1}	8×10^{-4} *

Table 2.2: A summary of variables and parameters including their typical values. * denotes a value given from [40, Figure 5], while † denotes a value that was estimated by inspecting [40] because it was not explicitly stated in [40, Figure 5].

Chapter 3

Numerical Methods and Comparison of Results

In this chapter we propose the following numerical methods for solving the spherically symmetric thermoregulation problem:

1. `WC`, a direct implementation of the method described by WC;
2. `FCI`, WC's method with an updated scheme for swarm radius $R(t)$;
3. and `ODE15S`, the previous method updated to use MATLAB's built-in solvers.

The schemes are discussed extensively in Section 3.3. We perform numerical simulations with each of the three methods to compare their results and offer recommendations on which approach is the best. We also discuss the biological and physical conclusions drawn from our simulations.

3.1 Computational Coordinate System

In this section, we discuss the basic spatial discretization used, which is based on a finite difference approach for a mapped radial coordinate system.

3.1.1 Mapped Coordinate System

As of now, our independent variables are t and r. For our computational domain, t varies from 0 to some final time t_f. On the other hand, for a fixed time, we have $r \in [0, R(t)]$, which means that a direct discretization of the governing equations has mesh points that move in time. To avoid this, we introduce a new dimensionless independent variable

$$x = \frac{r}{R(t)}, \tag{3.1}$$

and corresponding dependent variables

$$u(t,x) = T(t, r(t,x)), \tag{3.2}$$

$$v(t,x) = \rho(t, r(t,x)). \tag{3.3}$$

Hence, we need to transform Equations (2.1) and (2.3) into equations for u and v. After transforming the derivatives using the chain rule, the equations become

$$c\frac{\partial u}{\partial t} - \frac{cxR'}{R}\frac{\partial u}{\partial x} = \frac{1}{x^2R^2}\frac{\partial}{\partial x}\left[x^2\lambda\frac{\partial u}{\partial x}\right] + vf, \tag{3.4}$$

$$\frac{\partial v}{\partial t} - \frac{xR'}{R}\frac{\partial v}{\partial x} = \frac{1}{x^2R^2}\frac{\partial}{\partial x}\left[x^2\mu\frac{\partial v}{\partial x} - x^2\chi v\frac{\partial u}{\partial x}\right]. \tag{3.5}$$

For a complete derivation, see Appendix A.2.

Similarly, Equations (2.5) and (2.6) become

$$4\pi\int_0^1 x^2R(t)^3v(t,x)\mathrm{d}x = 0, \tag{3.6}$$

$$\frac{\mathrm{d}R}{\mathrm{d}t} = -\frac{\mu}{vR}\frac{\partial v}{\partial x} + \frac{\chi}{R}\frac{\partial u}{\partial x}\bigg|_{x=1}. \tag{3.7}$$

The transformation of the integral equation is described in Appendix A.3, while the derivation of the new differential equation (3.7) from the new integral equation (3.6) follows a similar argument to Appendix A.1.

Finally, the boundary conditions at the origin (Equations (2.7) and (2.8)) become

$$\frac{\partial u}{\partial x}\bigg|_{x=0} = 0, \tag{3.8}$$

$$\frac{\partial v}{\partial x}\bigg|_{x=0} = 0; \tag{3.9}$$

$$\tag{3.10}$$

while the exterior boundary conditions (Equations (2.9) and (2.10)) become

$$\frac{\partial u}{\partial x}\bigg|_{x=1} = -\frac{h_cR}{\lambda}(u - T_a)\bigg|_{x=1}, \tag{3.11}$$

$$v\big|_{x=1} = \rho_R. \tag{3.12}$$

3.1.2 Discretizing the Spatial and Temporal Variables

Our problem has both space and time dependence. In the dimensionless spatial coordinate system, we use N cells and $N+1$ grid points. We use a mesh that is uniform in space, so

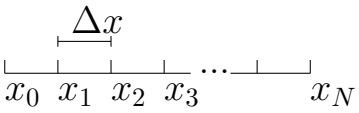

Figure 3.1: A visualization of the spatial mesh, with N cells and $N+1$ grid points. Moreover, as a result of rescaling r by $R(t)$, we must always have $x_0 = 0$ and $x_N = 1$.

our grid points are

$$x_i = i\Delta x, \tag{3.13}$$

where $\Delta x = \frac{1}{N}$ and $i = 0, 1, \ldots, N$. Hence a larger value of N corresponds to a finer computational grid. Notice that x_i has distance $i\Delta x$ from the origin. Figure 3.1 depicts the spatial discretization. For the time variable we simply choose some constant Δt, so that the nth time-step is denoted

$$t^n = n\Delta t. \tag{3.14}$$

Note that in some of our numerical methods, MATLAB automatically chooses a time-step and thus in this case we do not explicitly prescribe a time-step.

We now introduce notation to describe how we discretize the dependent variables. Suppose we have a function $g = g(t, x)$, then we denote its discrete approximations as

$$g_i^n \approx g(x_i, t^n).$$

In general, the subscript refers to a point in space, while the superscript refers to a point in time.

3.2 Finite Difference Approximation of Governing Equations

3.2.1 Temperature

Recall Equation (3.4)

$$c\frac{\partial u}{\partial t} - \frac{cxR'}{R}\frac{\partial u}{\partial x} = \frac{1}{x^2R^2}\frac{\partial}{\partial x}\left[x^2\lambda\frac{\partial u}{\partial x}\right] + vf.$$

We discretize the equation semi-implicitly in time by "freezing-coefficients," in which v, R, and the coefficients are evaluated at the previous time-step t^n, while u is evaluated at the next step t^{n+1}.

For space, suppose we know u_i^n for all i. We wish to have a discrete approximation for u_i^{n+1}. Firstly, we consider non-boundary terms ($i = 1, \ldots, N-1$) and examine each term in (3.4).

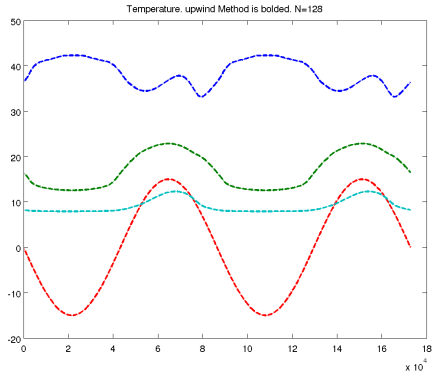

Figure 3.2: Using `ODE15S`, we calculate a solution using two finite differencing methods for the mesh advection term: an upwind scheme and a cell-centred scheme. The parameters used were those from Table 2.1, except $B = 16,244$.

For the time derivative, we use a forward difference approximation

$$\left(c\frac{\partial u}{\partial t}\right)_i \approx c\frac{u_i^{n+1} - u_i^n}{\Delta t}. \tag{3.15}$$

Regarding the mesh advection term, WC use an upwind scheme. However, we found that the difference between an upwind scheme and a centred scheme was negligible, as seen in Figure 3.2. Hence, for simplicity, we use a centred approximation

$$\left(\frac{cxR'}{R}\frac{\partial u}{\partial x}\right)_i \approx \frac{cx_i(R')^n}{R^n}\frac{u_{i+1}^{n+1} - u_{i-1}^{n+1}}{2\Delta x}. \tag{3.16}$$

We discuss how to approximate the coefficient R' in Section 3.2.4. To discretize the diffusion term, we use a cell-centred finite difference

$$\left(\frac{1}{x^2R^2}\frac{\partial}{\partial x}\left[x^2\lambda\frac{\partial u}{\partial x}\right]\right)_i \approx \frac{x_{i+\frac{1}{2}}^2\lambda_{i+\frac{1}{2}}^n(u_{i+1}^{n+1} - u_i^{n+1}) - x_{i-\frac{1}{2}}^2\lambda_{i-\frac{1}{2}}^n(u_i^{n+1} - u_{i-1}^{n+1})}{(R^n)^2x_i^2\Delta x^2}. \tag{3.17}$$

Notice that the dependent variables are evaluated at cell-edges, whereas the coefficients are located at the cell-centres. Hence interpolation is necessary for the coefficients. We use the exact value $x_{i+\frac{1}{2}} = (i + \frac{1}{2})\Delta x$ and the approximate value

$$\lambda_{i+\frac{1}{2}} \approx \frac{\lambda_{i+1} + \lambda_i}{2}.$$

Finally, the metabolic output is simply

$$(vf)_i \approx v_i^n f_i^n. \tag{3.18}$$

3.2.2 Bee Density

Recall Equation (3.5)

$$\frac{\partial v}{\partial t} - \frac{xR'}{R}\frac{\partial v}{\partial x} = \frac{1}{x^2R^2}\frac{\partial}{\partial x}\left[x^2\mu\frac{\partial v}{\partial x} - x^2\chi v\frac{\partial u}{\partial x}\right].$$

To solve for v_i^{n+1}, assume we know everything from time-step n and the temperature from time-step $n+1$. Similar discretizations to above for non-boundary terms ($i = 1, \ldots, N-1$) give

$$\left(\frac{\partial v}{\partial t}\right)_i \approx \frac{v_i^{n+1} - v_i^n}{\Delta t}, \tag{3.19}$$

$$\left(\frac{xR'}{R}\frac{\partial v}{\partial x}\right)_i \approx \frac{v_i(R')^n}{R^n}\frac{v_{i+1}^{n+1} - v_{i-1}^{n+1}}{2\Delta x}, \tag{3.20}$$

$$\left(\frac{1}{x^2R^2}\frac{\partial}{\partial x}\left[x^2\mu\frac{\partial v}{\partial x}\right]\right)_i \approx \frac{x_{i+\frac{1}{2}}^2\mu_{i+\frac{1}{2}}^n(v_{i+1}^{n+1} - v_i^{n+1}) - x_{i-\frac{1}{2}}^2\mu_{i-\frac{1}{2}}^n(v_i^{n+1} - v_{i-1}^{n+1})}{(R^n)^2x_i^2\Delta x^2}, \tag{3.21}$$

$$\left(\frac{1}{x^2R^2}\frac{\partial}{\partial x}\left[x^2\chi v\frac{\partial u}{\partial x}\right]\right)_i \approx \frac{x_{i+\frac{1}{2}}^2\chi_{i+\frac{1}{2}}^n v_{i+\frac{1}{2}}^n(u_{i+1}^{n+1} - u_i^{n+1}) - x_{i-\frac{1}{2}}^2\chi_{i-\frac{1}{2}}^n v_{i-\frac{1}{2}}^n(u_i^{n+1} - u_{i-1}^{n+1})}{(R^n)^2x_i^2\Delta x^2}. \tag{3.22}$$

3.2.3 Boundary Conditions

We now discuss the discretization of the boundary terms at the centre ($i = 0$) and the exterior ($i = N$).

Centre Boundary

Here we derive an equation for u_0^{n+1} given the solution at time n. The time derivative and shiver terms are similar to the non-boundary terms, and the mesh advection term is zero. The only term that behaves differently is the diffusive term which is undefined at $x = 0$ and thus must be treated carefully.

Expanding the diffusive term using the product rule for differentiation gives

$$\frac{1}{x^2}\frac{\partial}{\partial x}\left[x^2\lambda\frac{\partial u}{\partial x}\right] = \frac{2}{x}(\lambda u_x) + \frac{\partial}{\partial x}[\lambda u_x].$$

In the first term of the right-hand side, the numerator and denominator tend to zero as x tends to zero. So we apply L'Hôpital's rule to obtain

$$\left.\frac{1}{x^2R^2}\frac{\partial}{\partial x}\left[x^2\lambda\frac{\partial u}{\partial x}\right]\right|_{x=0} = \left.\frac{3}{R^2}\frac{\partial}{\partial x}[\lambda u_x]\right|_{x=0}, \tag{3.23}$$

which eliminates the problem with the factor of zero in the denominator. Applying centred-finite differences to this expression yields

$$\frac{3}{R^2}\frac{\partial}{\partial x}[\lambda u_x]\bigg|_{x=0} \approx \frac{3}{(R^n)^2}\frac{\lambda^n_{\frac{1}{2}}(u_1^{n+1}-u_0^{n+1})-\lambda^n_{-\frac{1}{2}}(u_0^{n+1}-u_{-1}^{n+1})}{\Delta x^2}.$$

We then use Equation (3.8) (derived from spherical symmetry) and get $u_{-1} = u_1$ and $\lambda_{-\frac{1}{2}} = \lambda_{\frac{1}{2}}$. Thus our approximation of the diffusion term at the origin is

$$\left(\frac{1}{x^2R^2}\frac{\partial}{\partial x}\left[x^2\lambda\frac{\partial u}{\partial x}\right]\right)_{i=0} \approx \frac{6\lambda^n_{\frac{1}{2}}(u_1^{n+1}-u_0^{n+1})}{(R^n)^2\Delta x^2}. \tag{3.24}$$

Similarly, for bee density, the time derivative term is the same as the non-boundary terms, the mesh advection term is zero, and the motility and thermotactic terms are approximated by

$$\left(\frac{1}{x^2R^2}\frac{\partial}{\partial x}\left[x^2\mu\frac{\partial v}{\partial x}\right]\right)_{i=0} \approx \frac{6\mu^n_{\frac{1}{2}}(v_1^{n+1}-v_0^{n+1})}{(R^n)^2\Delta x^2}, \tag{3.25}$$

$$\left(\frac{1}{x^2R^2}\frac{\partial}{\partial x}\left[x^2\chi v\frac{\partial u}{\partial x}\right]\right)_{i=0} \approx \frac{6\chi^n_{\frac{1}{2}}v^n_{\frac{1}{2}}(u_1^{n+1}-u_0^{n+1})}{(R^n)^2\Delta x^2}. \tag{3.26}$$

Exterior Boundary

For the boundary temperature u_N^{n+1}, the discrete equations are the same as those presented in Section 3.2.1 where we take $i = N$. This involves values of $x_{N+\frac{1}{2}}$, $\lambda_{N+\frac{1}{2}}$, and u_{N+1}^{n+1}, all of which need to be extrapolated from interior values. For x, we can simply use

$$x_{N+\frac{1}{2}} = x_N + \frac{\Delta x}{2}. \tag{3.27}$$

To approximate λ, we estimate $\Delta\lambda\big|_{x=1} \approx \lambda_N - \lambda_{N-1}$, giving the approximation

$$\lambda_{N+\frac{1}{2}} \approx \lambda_N + \frac{\lambda_N - \lambda_{N-1}}{2}. \tag{3.28}$$

For u_{N+1}, we use a second-order approximation

$$\left(\frac{\partial u}{\partial x}\right)_{i=N} \approx \frac{u_{N+1}-u_{N-1}}{2\Delta x},$$

and solve for u_{N+1} to obtain

$$u_{N+1} \approx u_{N-1} + 2\Delta x\frac{\partial u}{\partial x}\bigg|_{i=N}.$$

Moreover, discretizing Equation (3.11) gives

$$\left(\frac{\partial u}{\partial x}\right)_{i=N} \approx \frac{h_c R}{\lambda_N}(T_a - u_N). \tag{3.29}$$

Thus putting this all together gives the approximation

$$u_{N+1} \approx u_{N-1} + 2\Delta x \frac{h_c R}{\lambda_N}(T_a - u_N). \tag{3.30}$$

The ghost term u_{N+1} will appear for $i = N$ in Equations (3.16) and (3.17); in these cases we replaced u_{N+1} with the right-hand side of Equation (3.30).

For the density, we simply use the Dirichlet condition

$$v|_N = \rho_R. \tag{3.31}$$

3.2.4 Radius

We explore two different methods for approximating the swarm radius, $R(t)$. The first method is the one proposed by WC, where the differential equation (2.6) is used. The second method is a direct approximation of the original integral equation (2.5).

Differential Equation for Radius

This is the method described by WC. By approximating $\frac{\mathrm{d}R}{\mathrm{d}t}$ at each time-step, the radius can be updated using Forward Euler

$$R^{n+1} = R^n + \Delta t \frac{\mathrm{d}R}{\mathrm{d}t}^n. \tag{3.32}$$

To estimate $\frac{\mathrm{d}R}{\mathrm{d}t}$, recall Equation (3.7)

$$\frac{\mathrm{d}R}{\mathrm{d}t} = -\frac{\mu}{vR}\frac{\partial v}{\partial x} + \frac{\chi}{R}\frac{\partial u}{\partial x}\bigg|_{x=1}.$$

This gives an explicit equation for $\frac{\mathrm{d}R}{\mathrm{d}t}^n$

$$\frac{\mathrm{d}R}{\mathrm{d}t}^n \approx -\frac{\mu_N^n}{v_N^n R^n}\left(\frac{\partial v}{\partial x}\right)_N^n + \frac{\chi_N^n}{R^n}\left(\frac{\partial u}{\partial x}\right)_N^n, \tag{3.33}$$

where $\frac{\partial u}{\partial x}$ is computed by Equation (3.11)

$$\left(\frac{\partial u}{\partial x}\right)_N^n = \frac{h_c R^n}{\lambda_N^n}(T_a^n - u_N^n). \tag{3.34}$$

and $\frac{\partial v}{\partial x}$ is computed with a second order one-sided scheme

$$\left(\frac{\partial v}{\partial x}\right)_N^n = \frac{3v_N^n - 4v_{N-1}^n + v_{N-2}^n}{2\Delta x}. \tag{3.35}$$

Note that since u^{n+1} and v^{n+1} are computed before R in our frozen coefficients approach, then $\frac{\mathrm{d}R}{\mathrm{d}t}^{n+1}$ can be updated explicitly using u^{n+1} and v^{n+1}.

Integral Equation for Radius

It turns out that updating R using the approach just described has many computational difficulties (this will be discussed extensively in Section 3.3.2, and in Figure 3.4). As such, we derive an alternate approach to update R.

We can calculate the number of bees by integrating density over the sphere. Because of spherical symmetry, the number of bees $B(t)$ in the cluster at anytime t is given by

$$B(t) = 4\pi \int_0^{R(t)} r^2 \rho(t, r) \mathrm{d}r,$$

which on a normalized grid becomes

$$B(t) = 4\pi R(t)^3 \int_0^1 x^2 v(t, x) \mathrm{d}x \tag{3.36}$$

(see Appendix A.3 for the details). To discretize this integral, we use the trapezoidal rule to obtain

$$\begin{aligned}\int_0^1 x^2 v(t, x) \mathrm{d}x &\approx \frac{\Delta x}{2} \sum_{i=0}^{N-1} (x_i^2 v_i + x_{i+1}^2 v_{i+1}) \\ &= \Delta x \left(\sum_{i=1}^{N-1} x_i^2 v_i + \frac{1}{2} x_N^2 v_N \right),\end{aligned}$$

where $\Delta x = \frac{1}{N}$, N is the number of cells, and $x_i = i\Delta x$, for $i = 0, 1, \ldots, N$. Putting this all together and assuming we have a constant number of bees B_0 (and with Assumption 7, conservation of bees, in mind), we obtain the discrete equation

$$4\pi R^3 \Delta x \left(\sum_{i=1}^{N-1} x_i^2 v_i + \frac{1}{2} v_N \right) = B_0.$$

This can be rewritten as an explicit equation for $R(t)$

$$R(t) = \left(\frac{B_0}{4\pi\Delta x \left(\sum_{i=1}^{N-1} x_i^2 v_i + \frac{1}{2} v_N \right)} \right)^{\frac{1}{3}}, \tag{3.37}$$

which is easily computed once the values of v_i are known.

Coefficient R'

Notice that $R' = \frac{\mathrm{d}R}{\mathrm{d}t}$ appears as a coefficient in the upwinding terms for both u and v. We estimate this coefficient in two ways.

The first approximation is a direct application of Equation (3.33), which we demonstrate later introduces numerical difficulties (see Section 3.3 and Figure 3.4). We therefore propose a second approximation using Forward Euler

$$\frac{\mathrm{d}R^n}{\mathrm{d}t} = \frac{R^n - R^{n-1}}{\Delta t}. \tag{3.38}$$

3.2.5 Initial Conditions

Since we discretize our equations using a combination of forward and backward Euler time-stepping, we need an initial solution profile to proceed. That is, we require the initial conditions $R(0)$, and for all $r \in [0, R(0)]$ we require $T(0, r)$, and $\rho(0, r)$. WC do not describe their choice of initial conditions, and so we propose two options for creating initial conditions.

The first option is to take a constant temperature and density throughout the swarm. The density is taken as the Dirichlet boundary condition ρ_R to ensure the boundary condition is satisfied, while the temperature is more arbitrary (in practise, we choose a constant value from 20°C to 30°C). After picking a constant density, $R(0)$ is calculated to ensure that the radius is consistent with density. In particular, with a constant initial density ρ_R throughout the swarm, we require $R(0)$ to satisfy

$$B_0 = \frac{4\pi\rho_R}{3} R(0)^3. \tag{3.39}$$

The other method is slightly more sophisticated. After fixing the parameters of an experiment, we simulate a full period of the sinusoidal ambient temperature on a fine grid (i.e., number of grid points $N = 2^9$ or greater), then save the final temperature profile, density profile, and radius. These final profiles are then used as initial conditions for the next experiment using the same parameters. Note that for coarser grids (i.e., $N \leq 2^9$), we

interpolate values from the fine grid; in this case the radius is recalculated to ensure the correct number of bees.

3.3 Three Numerical Methods

To solve the discretized equations, we implemented three different methods into MATLAB. Here, we discuss the key differences between them.

3.3.1 Rescale Method, `WC`

This implementation is what we believe to be the method used by Watmough-Camazine based on the description in [40, Appendix]. We replicate their method as described in their appendix.

We use the method of freezing coefficients. We first solve for u by freezing v, R, and the coefficients λ and f at time t^n. This reduces the problem to inverting a tridiagonal matrix. Next, we compute v by freezing R and the coefficients μ, χ, and v at t^n, and using the updated u^{n+1}. Like u, solving for v is equivalent to inverting a tridiagonal matrix. Finally, R is solved using the differential equation (3.33). To ensure that Assumption 7 is satisfied, the number of bees is calculated using the updated v and R, and then the density is rescaled so that the number of bees is equal to the initial number of bees B_0. In particular, the following update is applied at every time-step:

$$v^{n+1} := \varsigma^{n+1} v^{n+1}, \tag{3.40}$$

where we have the *scale-factor* ς

$$\varsigma^{n+1} = \frac{B_0}{4\pi (R^{n+1})^3 \int_0^1 x^2 v^{n+1} \mathrm{d}x}. \tag{3.41}$$

Note because we derived $R(t)$ from the Assumption 7 (conservation of bees), we would have $\varsigma = 1$ at all time-steps if there was no error from numerics. The discretization of the PDEs is described in Section 3.2.

We refer to this method as `WC` to indicate that it is our attempt to reproduce the method presented by Watmough-Camazine in [40]. We also sometimes denote this method `rescale` to emphasize that at every time-step, the density profile needs to be rescaled to conserve the number of bees.

3.3.2 Updated Method, `FCI`

While the `WC` method gives seemingly physical results, the last step of rescaling the density profile to conserve bees is questionable. Without rescaling, the experiments exhibit *bee-drift*, where the number of bees grows quite rapidly. This causes the model to lose all

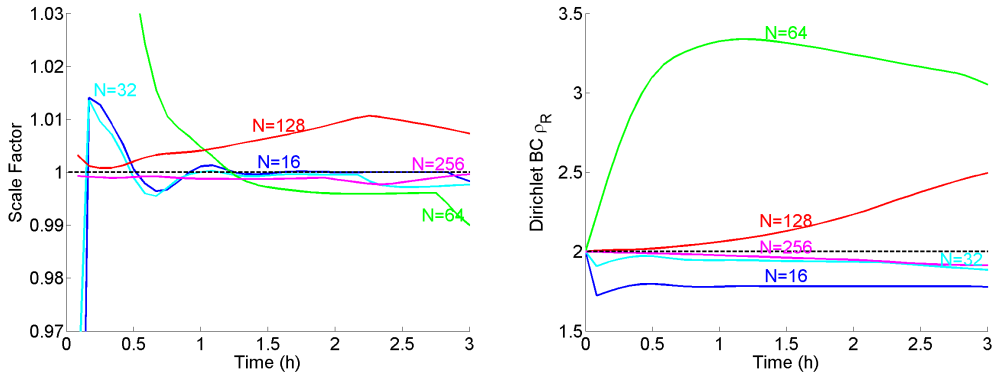

Figure 3.3: The scale-factor ς shows how much the density profile needs to be rescaled at every time-step (left). As a result of the rescaling, the Dirichlet boundary condition is also changing in time (right).

physical relevance because new bees are artificially introduced into the swarm. Assumption 7, conservation of bees, is built into the equations, and yet this assumption is clearly being violated. To remedy this problem, WC rescale the density profile by a factor of ς at every time-step, but this causes other problems.

In Figure 3.3, we demonstrate the effects of rescaling by plotting the scale-factor ς,which is a measure of the bee-drift. Since conservation of bees is built into the equations, we should always have $\varsigma = 1$ (i.e. no rescaling), yet clearly this is not the case. Note that if no rescaling is done, the number of bees can blow up to infinity. To make matters worse, the Dirichlet boundary condition (2.10) is also changing, meaning the Dirichlet boundary condition is changing arbitrarily in time - this makes little physical or computational sense.

We believe the cause of the drift is due to using the differential equation to compute $R(t)$, and thus we investigate this in Figure 3.4. Assuming forward Euler is close to correct, then with $N = 64$, $\frac{\mathrm{d}R}{\mathrm{d}t}$ computed with the differential equation often has the wrong magnitude; and by inspecting $R(t)$ vs t, it often has the wrong sign, a cause for alarm. Notice that upon refining the grid to $N = 128$, computing $\frac{\mathrm{d}R}{\mathrm{d}t}$ using either the differential equation or forward Euler makes little difference, as demonstrated by the overlapping plots.

With this in mind, we introduce a second numerical method to solve the equations. This method is identical to `WC` except for the way we compute R. Rather than using the differential equation (3.7), we use the integral equation (3.6), which eliminates the need to rescale the density to maintain the correct number of bees. Using the updated values of v and discretizing the integral with the trapezoidal rule, the following explicit equation is

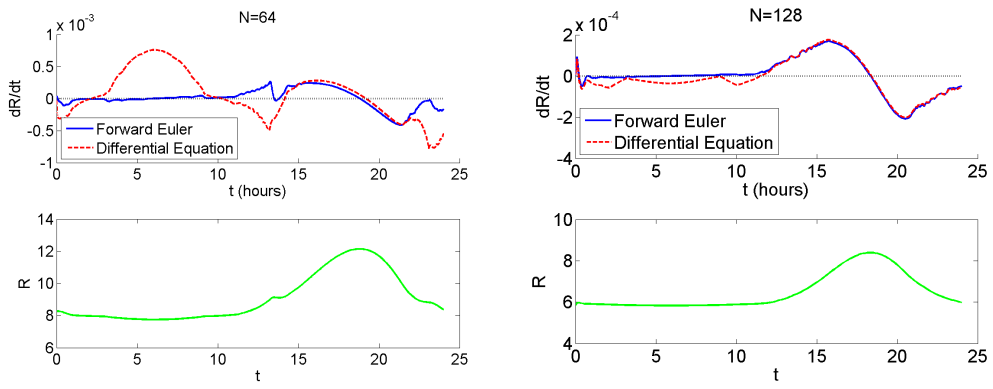

Figure 3.4: Swarm boundary speed coefficient $\frac{\mathrm{d}R}{\mathrm{d}t}$ computed using forward Euler and Equation (3.33). Note these calculations are made using method `FCI`, so $R(t)$ is computed with the integral equation (3.42); the differential equation is computed solely for comparison. Results are computed with $N = 64$ (left) and $N = 128$ (right) grid points.

used to compute $R(t)$

$$R(t) = \left(\frac{B_0}{4\pi\Delta x \left(\sum_{i=1}^{N-1} x_i^2 v_i + \frac{1}{2} v_N \right)} \right)^{\frac{1}{3}}, \tag{3.42}$$

which is derived in Section 3.2.4. We refer to this method as `FCI`, a shorthand for the method of freezing coefficients with the integral constraint.

3.3.3 MATLAB's Built-in Solvers, `ODE15S`

The previous two methods used semi-implicit time discretizations and frozen coefficients, whereas our third approach is an implicit approach in which u, v, and R are integrated in time simultaneously using MATLAB's built-in ODE-solvers. We use the same discretization as in `FCI`, but instead of freezing v and R to calculate u, all three are computed at the same time. Note that coefficients are still frozen at the previous time-step, including the coefficient v in the thermotactic term. Like `FCI`, R is computed using the integral equation (3.42), which upon discretization takes the form of an algebraic constraint. Thus we write a fully implicit scheme and let MATLAB's built-in function `ode15s` solve the equations. This method eliminates the need to prescribe a time-step Δt because `ode15s` automatically calculates Δt to satisfy prescribed error tolerances, which will drastically decrease the computation time.

Notice that in Equations (3.4) and (3.5), $\frac{\mathrm{d}R}{\mathrm{d}t}$ appears as a coefficient in the mesh advection term. Rather than using Equation (3.7) (which leads to problems, as demonstrated above), we edit MATLAB's built-in `ode15s` code to keep a global variable for $\frac{\mathrm{d}R}{\mathrm{d}t}$. We refer

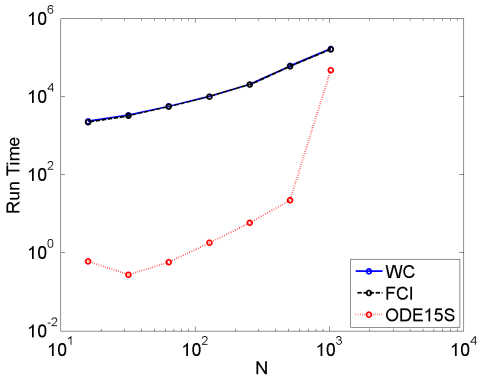

Figure 3.5: Computation time of the three methods, calculated using the built-in MATLAB `tic` and `toc` functions. The parameters used were those from Table 2.1 with $t_f = 3$ hours.

to this method as `ODE15S`. We emphasize that the lower-case `ode15s` refers to MATLAB's built-in solver, while `ODE15S` refers to our numerical method.

As demonstrated in Figure 3.5, the methods `WC` and `FCI` are typically over a hundred times slower than `ODE15S`. This is because `ode15s` does adaptive time-stepping, whereas the former two methods use a constant fixed Δt. Note the computation time in `WC` and `FCI` could be improved by picking a larger Δt, but this could introduce large time errors. In other words, picking a good time-step Δt is non-trivial, and thus using MATLAB's built-in time-stepping is a good idea.

3.4 Convergence Studies

We now perform several numerical convergence studies to ensure that our numerics are valid. We first demonstrate that each method is convergent (as $\Delta x \to 0$ and $\Delta t \to 0$), and then show that all three methods converge to the same result with the expected order of accuracy.

3.4.1 Individual Convergence

Here, we demonstrate each of our three methods is convergent without yet doing any explicit comparisons between one another. The parameter values used were the ones described in Table 2.1, where $t_f = 3$ hours.

To demonstrate numerical convergence in space, we first fix a scheme (`WC`, `FCI`, or `ODE15S`). We then compute the solution on a time-dependent problem (i.e. $T_{amp} \neq 0$) with a very fine spatial grid (number of cells $N = 2^9$ or $N = 2^{10}$) and take this as fine solution as the "true" solution. Then, with the same parameters (except N), we successively shrink Δx by taking larger values of N, (recall $\Delta x = \frac{1}{N}$). In particular, we take N

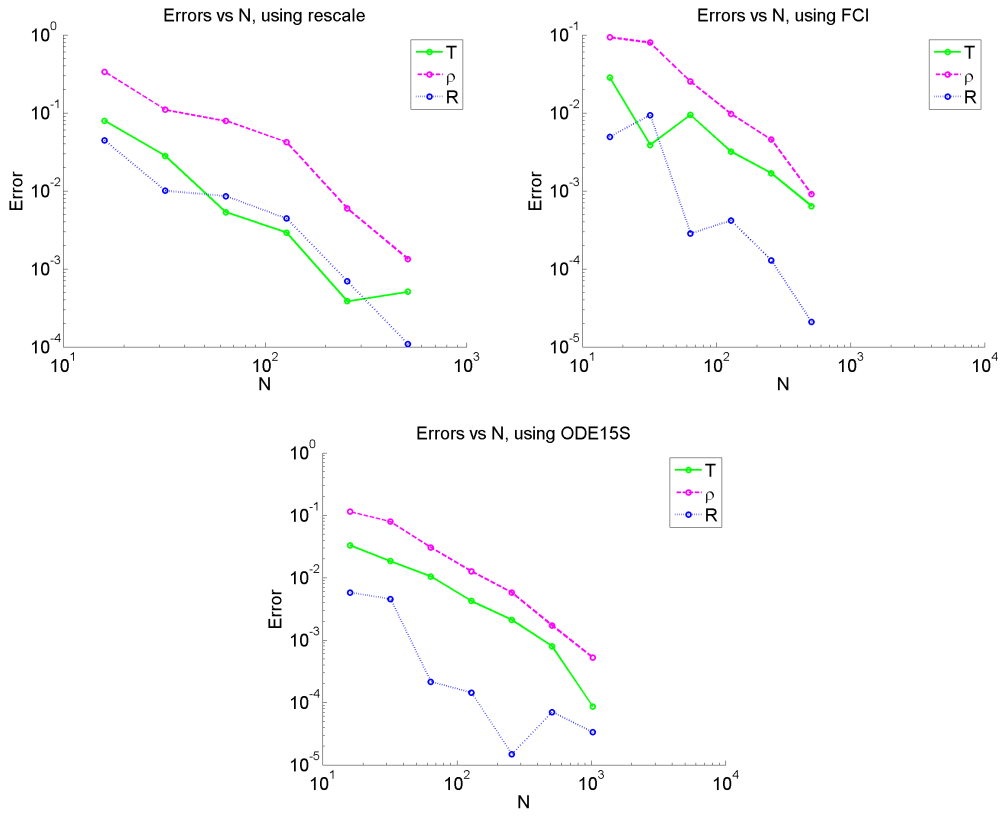

Figure 3.6: Error of the three methods plotted against the number of grid points for our three dependent variables. We simulated a time-dependent problem, then compared the final profiles.

as increasing powers of 2. We then choose Δt sufficiently small so that numerics are stable on the finest grid and hold Δt constant for all values of N.

We then compare the solution on each grid to the "true" solution at all points on the coarse grids (note that by construction, no interpolation is needed since the coarse grid points all coincide with fine grid points). To measure error, we use the ℓ^2-norm and normalize with respect to the number of grid points and the mean of the true value. The errors are plotted in Figure 3.6. Note that because R is scalar (i.e., has no N dependence) the convergence in space seems less regular than for u or v. This is probably the cause for the negative value in Table 3.1, and for the strange behaviour for convergence in Figure 3.6.

To estimate convergence rates, we take ratios of successive errors and take the logarithm (base 2, since N grows as powers of 2). This gives an approximation to the order of convergence, as seen in Table 3.1. The finite differencing is first order in time and second order in space, and the table shows that at least in v, the spatial convergence is in reasonable agreement with the expected second order.

	u	v	R
$\log_2\left(\frac{\text{Err}_{16}}{\text{Err}_{32}}\right)$	0.8435	0.5280	0.3483
$\log_2\left(\frac{\text{Err}_{32}}{\text{Err}_{64}}\right)$	0.8187	1.3643	4.4024
$\log_2\left(\frac{\text{Err}_{64}}{\text{Err}_{128}}\right)$	1.2985	1.2723	0.5735
$\log_2\left(\frac{\text{Err}_{128}}{\text{Err}_{256}}\right)$	0.9970	1.1280	3.2750
$\log_2\left(\frac{\text{Err}_{256}}{\text{Err}_{512}}\right)$	1.4151	1.7627	-2.2336
$\log_2\left(\frac{\text{Err}_{512}}{\text{Err}_{1024}}\right)$	3.2003	1.7055	1.0678

Table 3.1: Convergence rates of `ODE15S`. We use Err_N to denote the error of a solution using N points. The error was calculated using the ℓ^2-norm. The "true" solution is taken as the output using $N = 2048$.

3.4.2 Inter-Comparison of the Three Methods

Next, we demonstrate that all three methods converge to the same solution. The parameter values used were the ones described in Table 2.1, where $t_f = 3$ hours.

In Figure 3.7, by plotting final profiles in all three methods against x, we see that the profiles overlap as N increases. Note that the final radius R differs slightly between the three methods, especially for smaller N, which also means that the points in the physical domain are at different locations in space, which introduces additional errors in T and ρ. However, as N increases, the computed radii in all three methods become very close, and thus these additional errors become negligible.

We also give an ℓ^2-norm measure of the difference between `ODE15S` and the other two methods. We compare the final profile (u, v, and R) computed by `FCI` and `ODE15S` using the same N, and then observe how this difference changes as N increases. We repeat the experiment comparing `WC` with `ODE15S`. The results are plotted in Figure 3.8. We see that as N increases, the differences between the methods shrink. This is evidence for demonstrating that all three methods are indeed computing the same results.

3.4.3 Comparison to Watmough-Camazine

To demonstrate our code is a correct implementation of the method described in Watmough-Camazine's paper, we use the online applet *WebPlotDigitizer* [26] to extract the data presented in the original paper [40, Figure 5]. We computed a solution with `ODE15S` using the same parameters as those described under the figure, which are the parameters displayed in Table 2.1. We then plotted our results against the extracted data. To ensure the axes and scale are correct we compare the sinusoidal ambient temperature which is explicitly known – our ambient temperature overlapped exactly with the extracted data.

The results are presented in Figure 3.9. Our solution qualitatively matches the digitized plot in both the 8,104 bee and 16,244 bee simulations, and is quantitatively similar. It

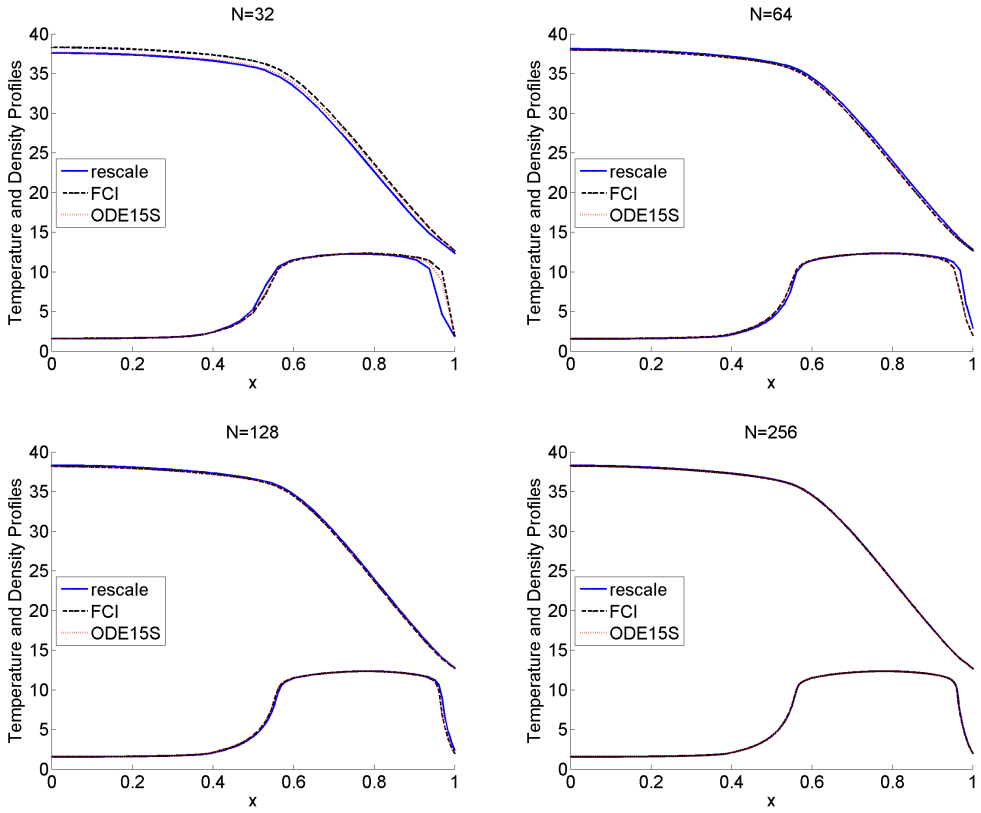

Figure 3.7: For various N, the final profiles are plotted against x, the non-dimensionalized distance from the centre of the cluster. For comparison, the results from all three methods are included in each graph.

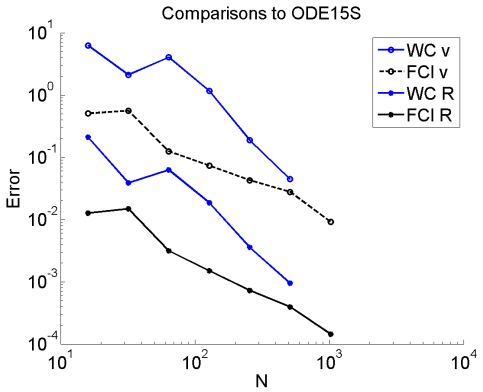

Figure 3.8: Comparisons between `FCI` (and `WC`) and `ODE15S`. We omit u as it is similar to v. As N increases, the difference between the methods shrink. Error is computed using the ℓ^2-norm.

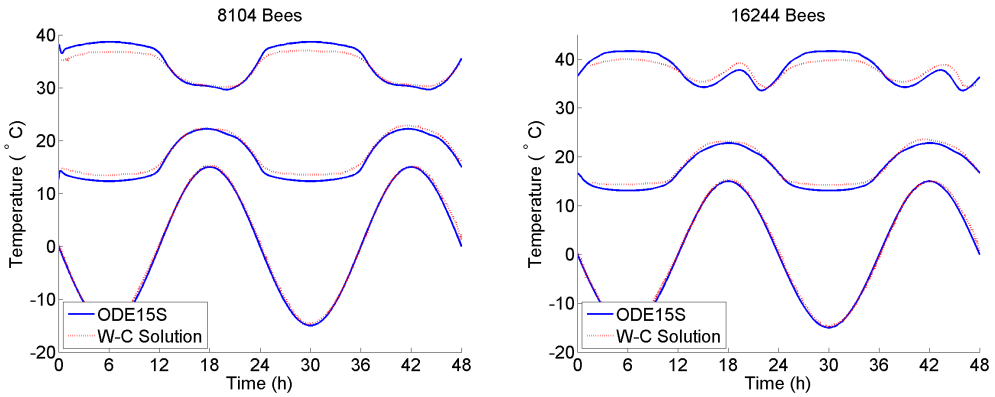

Figure 3.9: Plots extracted from Watmough-Camazine [40, Figure 5] and our replication of the results using `ODE15S`, using a swarm with 8,104 bees (left) and 16,244 bees (right). The top curve represents the innermost bees temperature, the second curve the outermost bees temperature, and the bottom curve the ambient temperature.

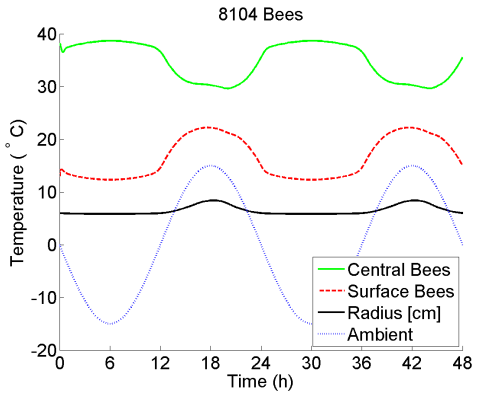

Figure 3.10: Similar to [40, Figure 5]. We chose to plot the radius alongside two of the most important locations of the swarm (the centre and exterior).

captures key features such as mean temperature, intervals of increase and decrease, and the strange hump seen in the 16,244 bee case. The cause for the differences is probably because of the unknown parameters T_m, T_s, and ρ_R.

3.5 Physical Results

We now discuss some physical interpretations of our model results, much of which follows the discussion presented in [40]. The results here are all simulated data generated from `ODE15S`, using parameter values from Table 2.1.

Figure 3.10 shows how the radius and the temperature at two key locations change in time. We simulate a small swarm with 8,104 bees, exposing them to a time-periodic ambient temperature. The results for the most part seem quite intuitive. A drop in ambient temperature causes the outermost bees' temperature to also drop; this should be expected

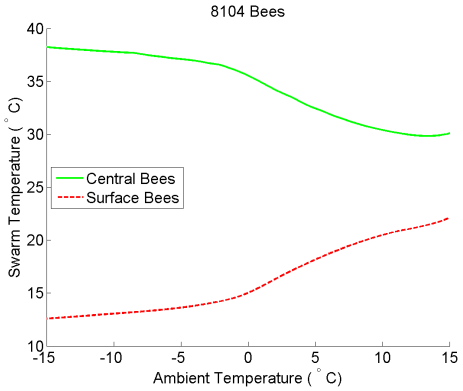

Figure 3.11: Similar to [40, Figure 6], temperature at the swarm centre and exterior vs ambient temperature.

since the outermost bees are in direct contact with the ambient air. Perhaps somewhat surprisingly though, as demonstrated in Figure 3.11, the ambient temperature is inversely related to the core temperature – that is, a drop in the ambient temperature causes an increase in core temperature, and vice versa. This inverse-relationship is observed in experimental data [14, 15]. Perhaps the best explanation for this lies in Figure 3.12, and the change in radius. A lower ambient temperature causes the bees to huddle closer to their neighbours, causing a thicker layer of bees to form near the swarm exterior. The thickening of bees reduces conductivity and hence helps trap heat on the inside, which is what causes the escalation in core temperature. Hence, this denser outer layer of bees acts as a thermally insulating layer.

For more details about the temperature and density profiles, we include heat-map plots in the sphere for the most interesting ambient temperatures (the extremes -15°C and 15°C, and 0°C), as seen in Figure 3.13. Notice that the swarm expands when the ambient temperature becomes warm. Moreover, in response to the cold, a thick layer of bees will form near the exterior.

For a more detailed discussion of the implications of this model, the reader is directed to [40, Section 4].

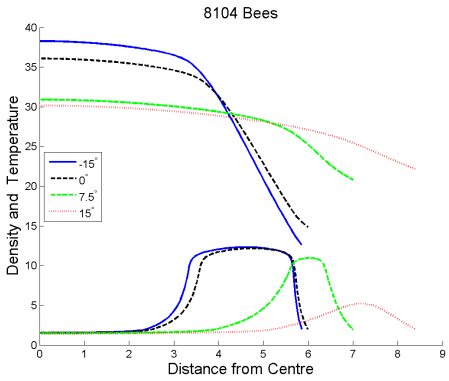

Figure 3.12: Similar to [40, Figure 8], temperature and density profiles for various ambient temperatures.

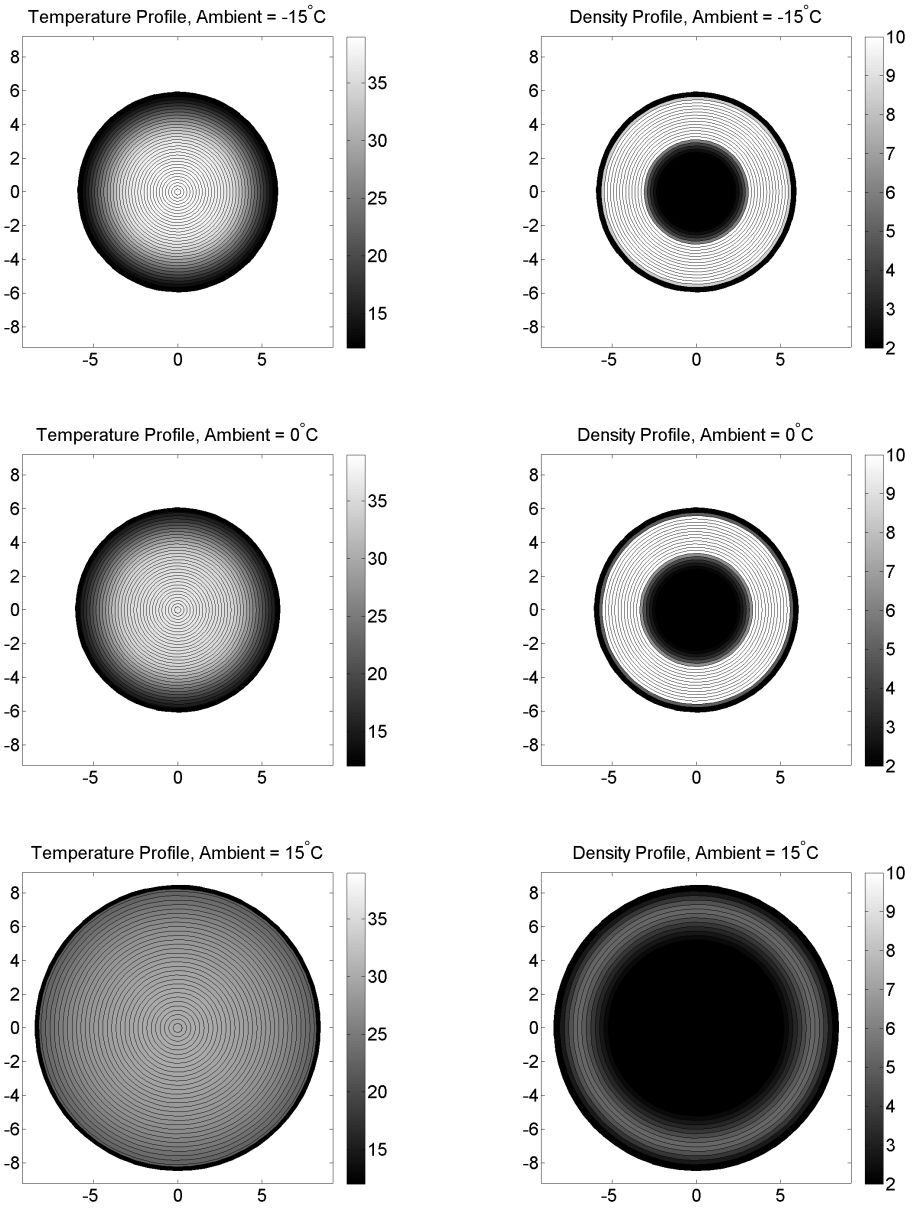

Figure 3.13: Temperature and density profiles for the most interesting ambient temperatures.

Chapter 4

Hemispherical Swarms

4.1 Problem Motivation

Assuming spherical symmetry significantly simplifies the mathematics of our problem, since it reduces the number of spatial dimensions from three to just one. However, physically this assumption oversimplifies the problem. As seen in Figures 1.1, 1.2, 4.1, and 4.2, the shape of swarms found in nature are not spherical. Furthermore, assuming that the bees are hanging from the upper-bounding surface (which we call the swarm *roof*) as a sphere means the swarm's point of contact with the roof is a single point, which would mean that a single bee is holding up the entire swarm. In addition to the problem with the shape, the effects of gravity and heat convection would also break the symmetry.

Many earlier models on the thermoregulation of honeybee swarms or winter clusters assume spherical symmetry, including [8, 20, 22, 24, 40]. The model presented by Ocko-Mahadevan [23] breaks spherical symmetry in the temperature field by including the effects of thermal buoyancy; however their model still assumes the swarm-shape is spherical.

In a paper published by Basak-Rao-Bejan [4], a model is presented to study a non-spherical swarm. The swarm's shape is imposed to match observations from [15, Figure 7].

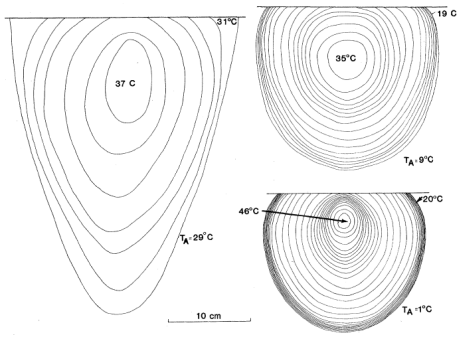

Figure 4.1: Image taken directly from [14, Figure 1] with permission. Contour plot of temperature for a swarm with 16,600 bees at three different ambient temperatures.

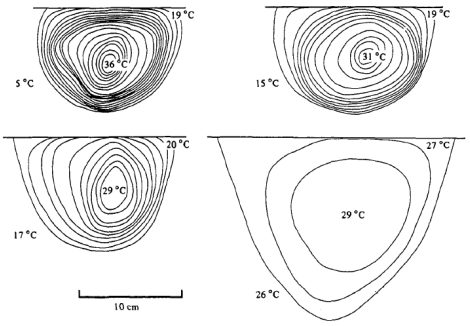

Figure 4.2: Image taken directly from [15, Figure 1] with permission. Contour plot of temperature for a swarm with 5,284 bees at four different ambient temperatures.

However, their model makes other non-physical simplifying assumptions. The density profile is taken as constant throughout the swarm. Also, the shape of the swarm is prescribed, and their discretization is handled in a case-by-case basis – that is, given an arbitrary cluster shape, the authors must manually create a mesh. We aim for a more robust numerical method.

Rather than using an Eulerian model, a Lagrangian model could be used to study swarms. A model that investigates non-spherical honeybee clusters is presented by Sumpter-Broomhead [37], where a winter cluster is studied using a Lagrangian model to allow the bees to move around the domain based on some attraction-repulsion assumptions. To ease the computation, they use only 100 bees in their standard colony, which is far fewer than the thousands of bees observed in real colonies [11, 30]. Fetecau-Guo [10] also use an agent based model to study honeybee swarming; in particular, they examine how a non-stationary honeybee swarm moves from the location of the stationary swarm to the selected nest site. Although they do not study the temperature of the swarm, their attraction-repulsion criteria for the locomotion of individual bees, along with their corresponding numerical methods which handles over 600 agents in a two-dimensional computational domain, could be adapted to our problem. We ultimately decided to avoid using an agent-based model because we would rather build on the existing continuum model we developed.

We aim to extend our model to break spherical symmetry while still maintaining cylindrical symmetry about the z-axis. As a first step, we assume that the swarm hanging from the roof is a hemisphere. Notice that the sketches of swarm-profiles from [14, 15], shown in Figures 4.1 and 4.2, are closer to semicircles than circles. Although going from a sphere to a hemisphere may seem like a trivial extension, there are significant changes to the model because the roof gives rise to different boundary conditions. Moreover, the numerics must be updated to handle two spatial dimensions. Note that the hemispherical shape simplifies many terms from the divergence and gradient in spherical coordinates. Bear in mind that by imposing the shape of a hemisphere, we are avoiding the issue of modelling exactly how a swarm's shape changes. Nonetheless, using a hemisphere is one step further toward

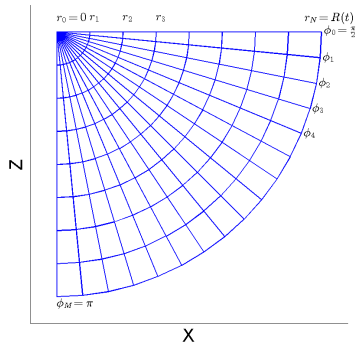

Figure 4.3: Semicircular computational domain. Rotational symmetry allows us to study a quarter-circle rather than a semicircle.

addressing this problem, and gives rise to many interesting changes from the spherically symmetric swarm.

4.2 Mathematical Formulation

Wherever applicable, we will use the same variables, governing equations, and constitutive functions from our one-dimensional model in Section 2.2.

4.2.1 Variables

We use t to denote time, and for space we use r as the distance from the origin, ϕ as the polar angle, and θ as the azimuthal angle. The azimuthal angle θ is dropped in most calculations due to rotational symmetry.

For our dependent variables, we use $T = T(t, r, \phi)$ for swarm temperature and $\rho = \rho(t, r, \phi)$ for bee density. We again use $R(t)$ to denote the radius of the semicircular swarm. Note that if we were to extend the model to non-spherical or non-hemispherical shapes, describing R as a "radius" no longer makes sense.

4.2.2 Computational Domain

We take the roof to correspond to the xy-plane. With rotational symmetry, it suffices to use spherical coordinates in a quarter-circle as the computational domain. Thus computationally, the swarm lies in the region $\theta = 0$, $\phi \in [\frac{\pi}{2}, \pi]$, and $r \in [0, R(t)]$. Note that if $R = R(t, \phi)$ (i.e. non-semicircular), then for a fixed ϕ we would have $r \in [0, R(t, \phi)]$. In Figure 4.3, we present the discretization of our computational domain, with more details provided in Section 4.4.2.

4.2.3 Equation for Temperature and Density

Recall Equation (2.1)

$$c\frac{\partial T}{\partial t} = \nabla \cdot (\lambda \nabla T) + \rho f,$$

where we now have $T = T(t, r, \phi)$. In spherical coordinates, with symmetry about θ, this becomes

$$c\frac{\partial T}{\partial t} = \frac{1}{r^2}\frac{\partial}{\partial r}\left[r^2\lambda\frac{\partial T}{\partial r}\right] + \frac{1}{r\sin\phi}\frac{\partial}{\partial \phi}\left[\frac{\lambda\sin\phi}{r}\frac{\partial T}{\partial \phi}\right] + \rho f. \tag{4.1}$$

Similarly, Equation (2.3)

$$\frac{\partial \rho}{\partial t} = \nabla \cdot (\mu(\rho)\nabla\rho) - \nabla \cdot (\chi(T)\rho\nabla T)$$

becomes

$$\begin{aligned}\frac{\partial \rho}{\partial t} = &\frac{1}{r^2}\frac{\partial}{\partial r}\left[r^2\mu\frac{\partial \rho}{\partial r}\right] + \frac{1}{r\sin\phi}\frac{\partial}{\partial \phi}\left[\frac{\mu\sin\phi}{r}\frac{\partial \rho}{\partial \phi}\right] \\ &- \frac{1}{r^2}\frac{\partial}{\partial r}\left[r^2\chi\rho\frac{\partial T}{\partial r}\right] + \frac{1}{r\sin\phi}\frac{\partial}{\partial \phi}\left[\frac{\chi\rho\sin\phi}{r}\frac{\partial T}{\partial \phi}\right].\end{aligned} \tag{4.2}$$

4.2.4 Equation for Hemispherical Swarm Radius

Similar to the one-dimensional case, we derive an equation for $R(t)$. Recall the formula to integrate a function $f(r, \phi, \theta)$ across the entire $\mathbb{R}^3$ space in spherical coordinates

$$\int_0^{2\pi}\int_0^{\pi}\int_0^{\infty} f(r,\phi,\theta)r^2\sin(\phi)\mathrm{d}r\mathrm{d}\phi\mathrm{d}\theta.$$

With initial number of bees B_0 and Assumption 7 (conservation of bees), integrating across the hemisphere for any fixed time yields

$$2\pi\int_{\frac{\pi}{2}}^{\pi}\left(\int_0^{R(t)}\rho(t,r,\phi)r^2\mathrm{d}r\right)\sin(\phi)\mathrm{d}\phi = B_0. \tag{4.3}$$

4.3 Boundary Conditions

We need to describe boundary conditions at the *interior* or *core* (which occurs at the z-axis, $\phi = \pi$), along the swarm *exterior* or *mantle* (which occurs at $r = R(t)$), and at the roof (which occurs in the xy-plane, $\phi = \frac{\pi}{2}$). See Figure 4.4 for a visualization of the boundaries. The interior and exterior of the swarm will have boundary conditions similar to the one-dimensional case, whereas the roof will need new conditions.

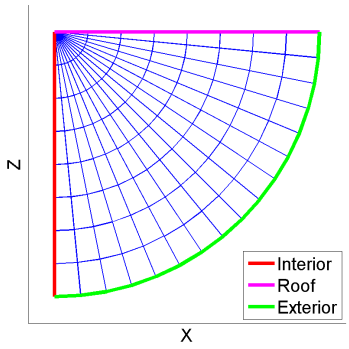

Figure 4.4: The three spatial boundaries in our computational domain.

4.3.1 Interior

For the interior boundary along $\phi = \pi$, rotational symmetry gives the boundary conditions

$$\frac{\partial T}{\partial \phi}(t, r, \pi) = 0, \tag{4.4}$$

$$\frac{\partial \rho}{\partial \phi}(t, r, \pi) = 0. \tag{4.5}$$

4.3.2 Exterior

Exterior Temperature - Newton's Law of Convective Heat Transfer

The temperature at the exterior is assumed to obey Newton's law of cooling. We have for fixed ϕ the Robin condition

$$\nabla T \cdot \vec{n}\Big|_{r=R} = \frac{h_c}{\lambda} \left(T_a(t) - T\right)\Big|_{r=R}, \tag{4.6}$$

where $\vec{n}$ is the outward normal. For a hemisphere, the outward normal is simply the vector from the origin to the exterior, thus

$$\frac{\partial T}{\partial r}(t, R(t), \phi) = \frac{h_c}{\lambda} \left(T_a(t) - T\right)\Big|_{r=R}. \tag{4.7}$$

Exterior Temperature - Dirichlet Condition

We will also sometimes use the temperature Dirichlet condition

$$T(t, R(t), \phi) = T_a(t). \tag{4.8}$$

Note that this is the boundary condition for temperature used in Ocko-Mahadevan's paper [23]. This may seem unreasonable since it allows the outermost bees to drop below

freezing temperatures which would rapidly kill them. However, in [23], T is defined as air temperature throughout the swarm, and in their model they allow the bees to be uncrowded at the mantle; hence the sparse mantle bees contribute little to the air temperature at the mantle. Moreover, in lab experiments from Heinrich [15], the recorded mantle temperature is not measured at the outermost extent of the swarm due to highly variable measurements there; rather it was measured directly underneath the outermost layer. This means that the recorded data from Heinrich does not actually report on the actual outermost bees, and that the mantle's temperatures are highly sporadic, and thus difficult to model correctly.

Exterior Density

For the exterior, the density is described by the Dirichlet condition

$$\rho(t, R(t), \phi) = \rho_R. \tag{4.9}$$

4.3.3 Roof

A novel aspect of our hemispherical swarm is considering how the swarm interacts with the roof. Note that we aim to compare our results to laboratory experiments presented in [14, 15] (see Figure 4.1). In [14], Heinrich does not describe in what type of vessel the captured swarm is contained in, and so we assume that he confined the swarm in a cylindrical Plexiglas container, which was what he used in the experiments from [15].

Roof Temperature

We now describe how heat is lost through the roof keeping in mind that Plexiglas is not a good insulator. Plexiglas's coefficient of thermal conductivity is assumed to be that of polymethyl methacrylate, which is 0.0017-0.0025 W $^\circ$C^{-1} cm^{-2} [7]. Thus we take the roof's coefficient of heat conductivity as $h_f = 0.002$ W $^\circ$C^{-1} cm^{-2}, which is roughly four times more conductive than λ_{bee}. Heinrich placed the Plexiglas containers into rooms and changed the ambient temperatures T_a, and thus Newton's law of cooling gives

$$\nabla T(t, r, \frac{\pi}{2}) \cdot \vec{n} = \frac{h_f}{\lambda(t, r)} \left(T_a(t) - T(t, r)\right) \Big|_{\phi=\frac{\pi}{2}}. \tag{4.10}$$

After computing the outward normal at the roof, which is discussed in Appendix B.1, we obtain

$$\frac{\partial T}{\partial \phi}\left(t, r, \frac{\pi}{2}\right) = -\frac{r h_f}{\lambda} \left(T_a(t) - T\right) \Big|_{\phi=\frac{\pi}{2}}. \tag{4.11}$$

Roof Density

The bee density at the roof is uncertain because of a lack of experimental results. One choice is to use a Dirichlet condition

$$\rho(t, r, \frac{\pi}{2}) = \rho_f, \tag{4.12}$$

where ρ_f would be some chosen value. This boundary condition is similar to how the density is described at the exterior mantle. However, as observed in [14, Figure 1], unlike the somewhat uniform temperature across the swarm mantle, the temperature at the roof varies greatly between the interior and exterior of the swarm. Hence assuming the bees are uniform across the roof seems inappropriate, especially since our numerical results from before demonstrate that densities will vary as the temperature changes.

As such, we use the no-flux boundary condition

$$\frac{\partial \rho}{\partial \phi}(t, r, \frac{\pi}{2}) = 0. \tag{4.13}$$

This seems fitting since bees cannot leave the swarm through the roof, and also allows for the bees to move along the roof to adapt to the local temperature changes.

4.4 Hemispherical Computational Coordinate System

In this section, we discuss the spatial discretization used, which is based on a finite difference approach for a mapped spherical coordinate system with rotational symmetry.

4.4.1 Mapped Coordinate System

Similar to the one-dimensional case, a direct discretization of $r \in [0, R(t)]$ will result in moving mesh points, and hence we introduce the dimensionless computational coordinate

$$x = \frac{r}{R(t)}. \tag{4.14}$$

We also introduce the corresponding dependent variables

$$u(t, x, \phi) = T(t, r(t, x), \phi), \tag{4.15}$$

$$v(t, x, \phi) = \rho(t, r(t, x), \phi). \tag{4.16}$$

Transformed Governing Equations

We need to transform the equations for T and ρ (Equations (4.1) and (4.2)) into corresponding equations for u and v. In Appendix C.1, we derive the transformations for these equations in general convex two-dimensional domains. The hemisphere is a special case of

this and hence the transformation we seek comes from setting $P = \frac{\partial R}{\partial \phi} = 0$ in Equations (C.12) and (C.13). Thus we have the new equation for temperature

$$\begin{aligned} c\frac{\partial u}{\partial t} - c\frac{x\dot{R}}{R}\frac{\partial u}{\partial x} =& \frac{1}{x^2R^2}\frac{\partial}{\partial x}\left[x^2\lambda\frac{\partial u}{\partial x}\right] \\ &+ \frac{1}{xR\sin\phi}\frac{\partial}{\partial \phi}\left[\frac{\lambda\sin\phi}{xR}\frac{\partial u}{\partial \phi}\right] + vf, \end{aligned} \tag{4.17}$$

and for density

$$\begin{aligned} \frac{\partial v}{\partial t} - \frac{x\dot{R}}{R}\frac{\partial v}{\partial x} =& \frac{1}{x^2R^2}\frac{\partial}{\partial x}\left[x^2\mu\frac{\partial v}{\partial x} - x^2\chi v\frac{\partial u}{\partial x}\right] \\ &+ \frac{1}{xR\sin\phi}\frac{\partial}{\partial \phi}\left[\frac{\mu\sin\phi}{xR}\frac{\partial v}{\partial \phi} - \frac{\chi v\sin\phi}{xR}\frac{\partial u}{\partial \phi}\right]. \end{aligned} \tag{4.18}$$

Beginning from Equation (4.3), a derivation similar to the work in Appendix A.3 gives

$$2\pi\int_{\frac{\pi}{2}}^{\pi}\left(\int_0^1 v(t,x,\phi)x^2R(t)^3\mathrm{d}x\right)\sin(\phi)\mathrm{d}\phi = B_0. \tag{4.19}$$

Transformed Boundary Conditions

We also transform the boundary conditions. At the interior, Equations (4.4) and (4.5) become

$$\frac{\partial u}{\partial \phi}(t,x,\pi) = 0, \tag{4.20}$$

$$\frac{\partial v}{\partial \phi}(t,x,\pi) = 0. \tag{4.21}$$

At the exterior, Equations (4.7) and (4.9) become

$$\frac{\partial u}{\partial x}(t,1,\phi) = \frac{h_cR(t)}{\lambda}\left(T_a(t) - u\right)\Big|_{x=1}, \tag{4.22}$$

$$v(t,1,\phi) = \rho_R. \tag{4.23}$$

At the roof, Equations (4.11) and (4.13) become

$$\frac{\partial u}{\partial \phi}\left(t,x,\frac{\pi}{2}\right) = -\frac{xR(t)h_f}{\lambda}\left(T_a(t) - u\right)\Big|_{\phi=\frac{\pi}{2}}. \tag{4.24}$$

$$\frac{\partial v}{\partial \phi}\left(t,x,\frac{\pi}{2}\right) = 0. \tag{4.25}$$

4.4.2 Discretizing the Spatial and Temporal Variables

We use N and M to respectively denote the number of grid points in x and ϕ. Our grid points will lie on

- $x_i = i\Delta x$, where $\Delta x = \frac{1}{N}$ and $i = 0, \ldots, N$,
- $\phi_j = j\Delta\phi$, where $\Delta\phi = \frac{\frac{\pi}{2}}{M}$ and $j = 0, \ldots, M$.

Figure 4.3 depicts the discretized mesh. For the temporal discretization, the nth time-step is denoted t^n. In general, the discretization in time is not uniform because MATLAB uses adaptive time-stepping.

To describe the discretization of dependent variables, suppose we have a function $g(t, x, \phi)$. We denote its discretization as

$$g_{i,j}^n \approx g(t^n, x_i, \phi_j). \tag{4.26}$$

In general, the superscript refers to a point in time, the subscript i refers to a distance from the origin, and the subscript j refers to a ray. At $i = 0$, which corresponds to the origin, there is no j dependence, and hence for all $j = 0, \ldots, M$, we denote

$$g_0 = g_{0,j}. \tag{4.27}$$

4.5 Finite Difference Approximation of Governing Equations

In this section, we discuss the finite difference approximations of our governing equations. We will again use a modified version of MATLAB's `ode15s`. The following approximations are similar to those from Section 3.2.

4.5.1 Temperature and Density

Recall Equation (4.17)

$$\begin{aligned} c\frac{\partial u}{\partial t} - c\frac{x\dot{R}}{R}\frac{\partial u}{\partial x} =& \frac{1}{x^2R^2}\frac{\partial}{\partial x}\left[x^2\lambda\frac{\partial u}{\partial x}\right] \\ &+ \frac{1}{xR\sin\phi}\frac{\partial}{\partial\phi}\left[\frac{\lambda\sin\phi}{xR}\frac{\partial u}{\partial\phi}\right] + vf. \end{aligned}$$

We first discretize non-boundary terms (so $i \neq 0, N$ and $j \neq 0, M$). The mesh advection term could be approximated with an upwinding scheme, but instead we use a cell-centred difference scheme for simplicity (see Figure 3.2 for a brief discussion on this) and obtain

$$\left(-c\frac{x\dot{R}}{R}\frac{\partial u}{\partial x}\right)_{i,j} \approx -c\frac{x_i\dot{R}}{R}\frac{u_{i+1,j} - u_{i-1,j}}{2\Delta x}. \tag{4.28}$$

The $\frac{\partial}{\partial x}\frac{\partial}{\partial x}$ diffusion term becomes

$$\left(\frac{1}{x^2R^2}\frac{\partial}{\partial x}\left[x^2\lambda\frac{\partial u}{\partial x}\right]\right)_{i,j} \approx \frac{1}{x_i^2R^2}\left(\frac{x^2_{i+\frac{1}{2}}\lambda_{i+\frac{1}{2},j}}{\Delta x^2}(u_{i+1,j}-u_{i,j}) - \frac{x^2_{i-\frac{1}{2}}\lambda_{i-\frac{1}{2},j}}{\Delta x^2}(u_{i,j}-u_{i-1,j})\right). \tag{4.29}$$

The $\frac{\partial}{\partial \phi}\frac{\partial}{\partial \phi}$ diffusion term becomes

$$\left(\frac{1}{xR\sin\phi}\frac{\partial}{\partial\phi}\left[\frac{\lambda\sin\phi}{xR}\frac{\partial u}{\partial\phi}\right]\right)_{i,j} \approx \frac{1}{x_iR\sin\phi_j}\left(\gamma_{i,j+\frac{1}{2}}(u_{i,j+1}-u_{i,j}) - \gamma_{i,j-\frac{1}{2}}(u_{i,j}-u_{i,j-1})\right), \tag{4.30}$$

where

$$\gamma_{i,j} = \frac{\sin\phi_j\lambda_{i,j}}{x_iR\Delta\phi^2}. \tag{4.31}$$

Finally, the source term is simply

$$(vf)_{i,j} = v_{i,j}f_{i,j}. \tag{4.32}$$

The finite difference approximation for bee density v is similar to the temperature's approximation and thus omitted here.

4.5.2 Boundary Conditions

Above we derived finite difference approximations for non-boundary terms. At the boundaries, the boundary conditions must be applied for certain terms. Moreover, the origin involves a coordinate singularity which must be resolved.

Interior

In the interior ($j = M$) for both u and v, the mesh advection term, the x-diffusion term, and the source term are treated like non-boundary terms. However, the ϕ-diffusion term is undefined at $\phi = \pi$ because there is a $\sin\phi$ in the denominator. For temperature u, as demonstrated in Appendix C.2, in the limit as $\phi \to \pi$ we obtain

$$\frac{1}{x^2R\sin\phi}\frac{\partial}{\partial\phi}\left[\sin\phi\frac{\lambda u_\phi}{R}\right]\Bigg|_{\phi=\pi} = \frac{2}{x^2R^2}\frac{\partial}{\partial\phi}\left[\lambda\frac{\partial u}{\partial\phi}\right]\Bigg|_{\phi=\pi}.$$

Hence aside from the origin ($i = 0$), we have

$$\left(\frac{1}{x^2 R \sin\phi}\frac{\partial}{\partial\phi}\left[\sin\phi\frac{\lambda u_\phi}{R}\right]\right)_{i,M} \approx \frac{4\lambda_{i,M-\frac{1}{2}}}{x_i^2 R^2 \Delta\phi^2}(u_{i,M-1} - u_{i,M}) \tag{4.33}$$

The boundary condition for density v is similar.

Exterior

For the temperature, consider $i = N$ and any j. The mesh advection term and x-diffusion term will involve $u_{N+1,j}$, which needs to be approximated. We use the second-order approximation

$$u_{N+1,j} \approx u_{N-1,j} + 2\Delta x\left(\frac{\partial u}{\partial x}\right)_{N,j}, \tag{4.34}$$

where discretizing Equation (4.22) gives

$$\left(\frac{\partial u}{\partial x}\right)_{N,j} \approx \frac{h_c R}{\lambda_{i,j}}(T_a - u_{N,j}). \tag{4.35}$$

For the density, we have for any j the Dirichlet condition

$$v_{N,j} = \rho_R. \tag{4.36}$$

Roof

At the roof, a direct application of Equation (4.30) for u's ϕ-diffusion term would involve $u_{i,-1}$, $\lambda_{i,-\frac{1}{2}}$, and $\sin\phi_{-\frac{1}{2}}$, which are points outside of our coordinate system. To approximate $u_{i,-1}$, we use a second-order approximation to obtain

$$u_{i,-1} = u_{i,1} - 2\Delta\phi\left.\frac{\partial u}{\partial\phi}\right|_{i,0}, \tag{4.37}$$

where discretizing Equation (4.11) gives

$$\left(\frac{\partial u}{\partial\phi}\right)_{i,0} \approx -\frac{x_i R h_f}{\lambda_{i,0}}(T_a - u_{i,0}). \tag{4.38}$$

To approximate λ, we estimate $\Delta\lambda\big|_{i,0} = \lambda_{i,1} - \lambda_{i,0}$, giving the approximation

$$\lambda_{i,-\frac{1}{2}} \approx \lambda_{i,0} - \frac{\lambda_{i,1} - \lambda_{i,0}}{2}. \tag{4.39}$$

Moreover, symmetry of the sine function across $\phi = \frac{\pi}{2}$ yields

$$\sin\phi_{-\frac{1}{2}} = \sin\phi_{\frac{1}{2}}. \tag{4.40}$$

Similarly, the density ϕ-diffusion term will involve points outside our coordinate system. However, due to the symmetrical boundary condition Equation (4.50), we have

$$v_{i,-1} = v_{i,1}, \tag{4.41}$$

$$v_{i,-\frac{1}{2}} = v_{i,\frac{1}{2}}, \tag{4.42}$$

$$\mu_{i,-\frac{1}{2}} = \mu_{i,\frac{1}{2}}. \tag{4.43}$$

Origin

The origin in spherical coordinates needs to be treated with much care due to the coordinate singularity. We follow a method similar to the discretization of the origin in polar coordinates presented by Strikwerda [36]. The derivation of our approximation of the origin in spherical coordinates is presented in Appendix B.2 where we derive Equation (B.12). Upon transformation into the mapped coordinate system (noting that the mesh advection term is zero at the origin), this equation gives an approximation to the time-derivative at the origin

$$\left(\frac{\partial u}{\partial t}\right)_{i=0} \approx \frac{6\Delta\phi}{\Delta x^2 R^2} \sum_{j=1}^{M} \sin\phi_j \lambda_{\frac{1}{2},j}(u_{1,j} - u_0) + v_0 f_0. \tag{4.44}$$

Similarly for density, we have the approximation

$$\left(\frac{\partial v}{\partial t}\right)_{i=0} \approx \frac{6\Delta\phi}{\Delta x^2 R^2} \sum_{j=1}^{M} \sin\phi_j \left(\mu_{\frac{1}{2},j}(v_{1,j} - v_0) - \chi_{\frac{1}{2},j} v_{\frac{1}{2},j}(u_{1,j} - u_0)\right). \tag{4.45}$$

4.5.3 Swarm Radius

To approximate the radius, we directly discretize the integral equation (4.19) using trapezoidal rule. In Appendix C.3 we derive a discretization for swarms more general than a hemisphere. Since the hemisphere is a special case of Equation (C.19) where R has no ϕ dependence, we have

$$B_0 = 2\pi\Delta x\Delta\phi \sum_{i=0}^{N} c_i x_i^2 \sum_{j=0}^{M} \tilde{c}_j \sin(\phi_j) R^3 v_{i,j}, \tag{4.46}$$

where we have trapezoidal integration constants

$$c_i = \begin{cases} \frac{1}{2}, & \text{if } i = 0, N, \\ 1, & \text{if } i \neq 0, N, \end{cases} \tag{4.47}$$

$$\tilde{c}_j = \begin{cases} \frac{1}{2}, & \text{if } j = 0, M, \\ 1, & \text{if } j \neq 0, M. \end{cases} \tag{4.48}$$

Solving for R gives the approximation

$$R = \left(\frac{B_0}{2\pi \Delta x \Delta \phi \sum_{i=0}^{N} c_i x_i^2 \sum_{j=0}^{M} \tilde{c}_j \sin(\phi_j) v_{i,j}} \right)^{\frac{1}{3}}. \tag{4.49}$$

4.6 Numerical Simulations of a Hemispherical Swarm

Before we present simulations of our hemispherical swarm model, we perform a numerical convergence study to validate the numerical method. Since we have already undergone numerous convergence studies with our one-dimensional numerical scheme, we will compare the two-dimensional results with equivalent one-dimensional simulations whenever possible. Unless otherwise stated, the parameter values are those from Table 2.1.

4.6.1 Spherically Symmetric Case

To validate the two-dimensional numerical scheme, we impose boundary conditions at the roof that make the problem spherically symmetric. This allows us to directly compare our two-dimensional results to the one-dimensional results. In particular, the roof boundary conditions at the roof are taken as

$$\frac{\partial T}{\partial \phi}(t, r, \frac{\pi}{2}) = 0, \tag{4.50}$$

$$\frac{\partial \rho}{\partial \phi}(t, r, \frac{\pi}{2}) = 0. \tag{4.51}$$

Note that the density no-flux roof boundary condition (Equation (4.13)) is the same as the symmetry condition here.

Temperature Dirichlet Condition at the Exterior

We first use the temperature Dirichlet condition Equation (4.8) at the exterior because it is simpler to implement than the Robin condition. We make the ambient temperature non-oscillatory (i.e. $T_{amp} = 0$) with $T_{mean} = 15$, then simulate to steady state using the one-dimensional `ODE15S` (modified to accommodate the new boundary condition), which we have already verified is correct. Using the same parameters, we then run several experiments using the hemispherical code for various N and M.

As expected, spherical symmetry was observed in the two-dimensional solution at steady state, evidenced by there being no variation across different rays. Thus we chose the rays corresponding to $j = 0$ to compare to the "correct" one-dimensional solution. Upon refinement of the mesh, the final solution profiles of the two-dimensional simulation quickly overlap with the "correct" simulation, as seen in Figure 4.5. To demonstrate convergence in

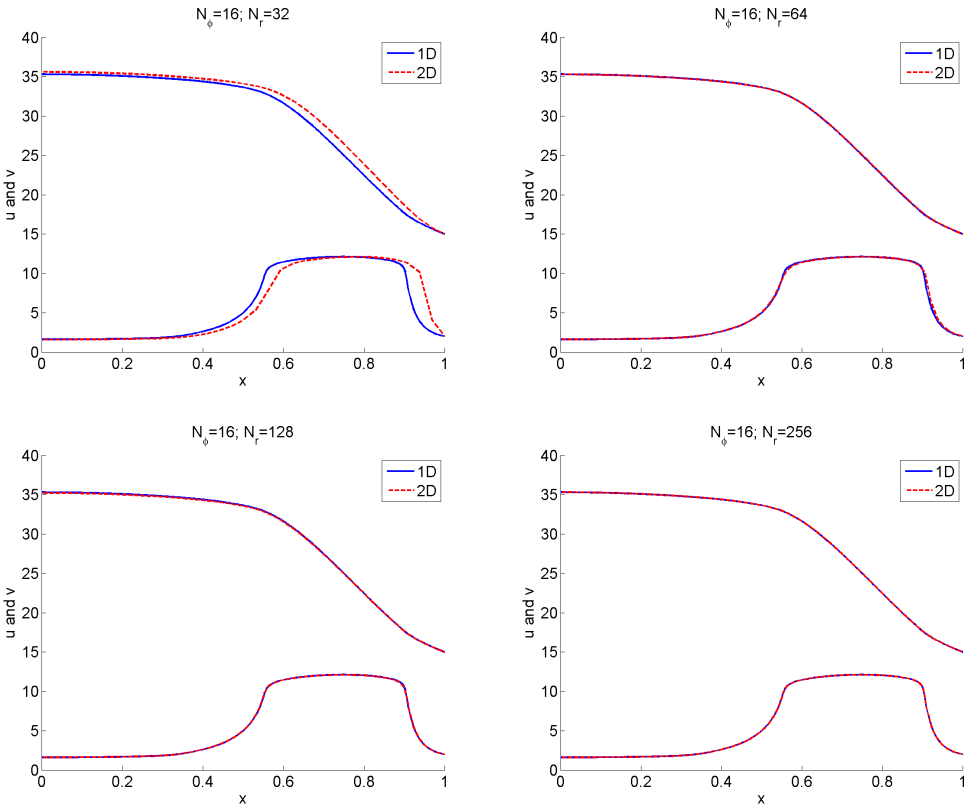

Figure 4.5: Final profiles, where we fix $M = 16$ and increase N. The roof uses reflexive boundary conditions, while the exterior uses the Dirichlet condition for u.

time, Figure 4.6 shows how the temperature changes in time for the fixed radial locations $x = 0$, 0.25, 0.5, and 0.75. The exterior $x = 1$ is omitted because the Dirichlet conditions for temperature and density are implemented exactly with no discretization error. We plotted solution profiles for successively larger values of N and found the two-dimensional simulations converged to the one-dimensional result. Somewhat surprisingly, radial points near the origin exhibited less error than near the exterior.

Error is shown as a function of both N and M in Figure 4.7. The correct solution was taken as the solution from the one-dimensional code using $N = 256$. Notice that refining $\Delta\phi$ does little, which is a result of the symmetry across ϕ. Most importantly, refinements in Δx lead to errors clearly tending toward zero.

Temperature Robin Condition at the Mantle

We now investigate the spherically symmetric case with the Robin mantle condition (4.7). We revert back to comparing steady state solutions by choosing $T_{mean} = 0$ and $T_{amp} = 15$. We again use `ODE15S` to compute a solution using $N = 256$ and take this as the "correct" solution, then compute several solutions in two-dimensions with varying N and M.

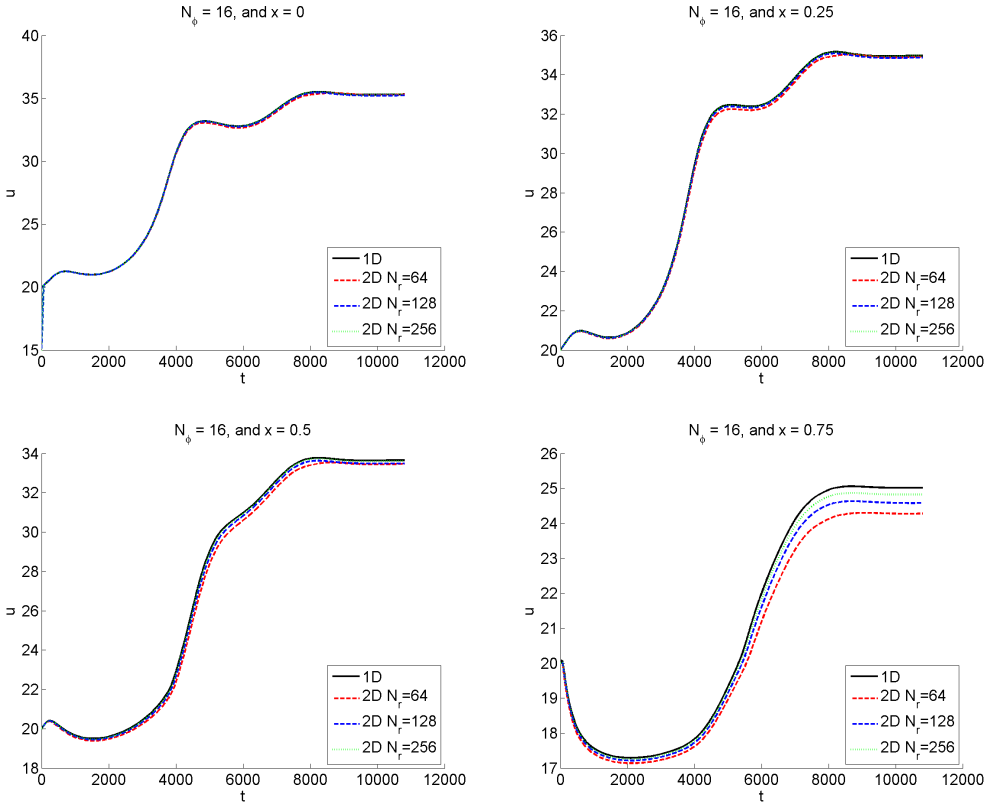

Figure 4.6: For fixed radial locations and various grid resolutions, we examine the temperature's time-dependence. We use a fixed M and various N. The roof uses reflexive boundary conditions, while the exterior uses the Dirichlet condition for u.

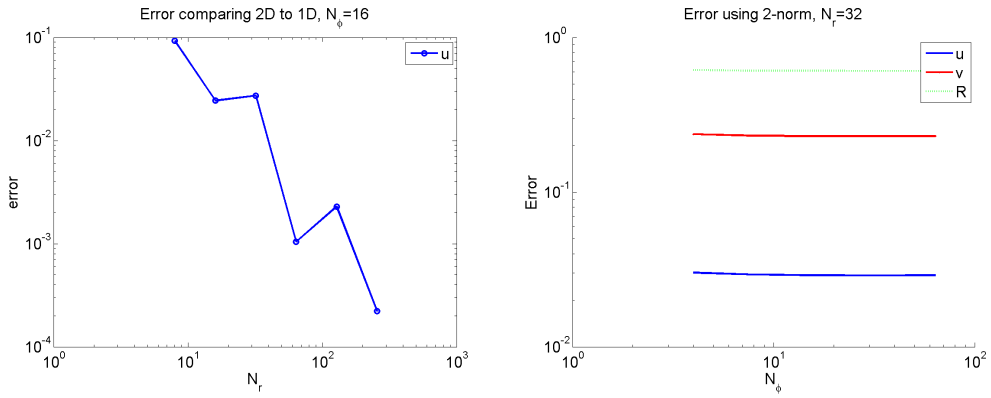

Figure 4.7: Error of final profiles with the ℓ^2-norm in the spherically symmetric two-dimensional code compared to the one-dimensional solution with $N = 256$. In the left we fix $M = 16$ and increase N, while in the right we fix $N = 32$ and increase M. The roof uses reflexive boundary conditions, while the exterior uses the Dirichlet condition for u.

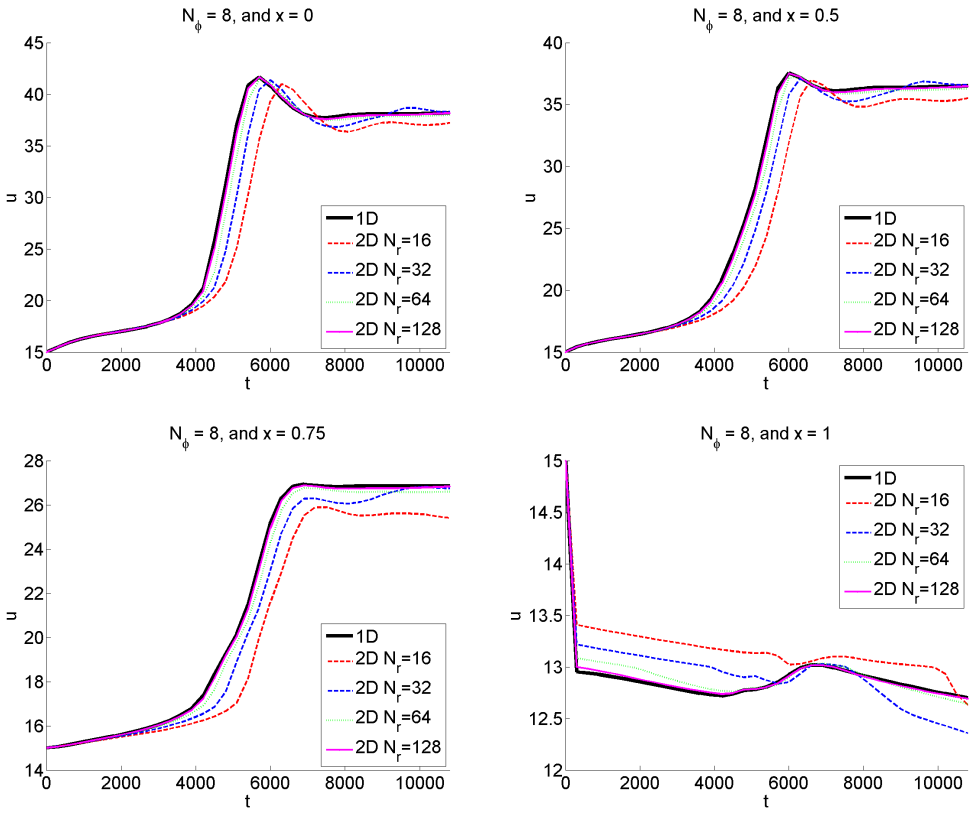

Figure 4.8: For fixed radial locations and various grid resolutions, we examine the temperature's time-dependence with a fixed M and various N. The roof uses reflexive boundary conditions, while the exterior uses the Robin condition for u.

We see in Figure 4.8 that the solutions match in time. For multiple N and fixed locations in space, notice that the time profiles with $N = 128$ overlap very well with the one-dimensional solution. The error rate as a function of N is demonstrated in Figure 4.9. We found refinements in M quickly did little due to the spherical symmetry. The error is calculated by comparing the final solution profiles with the "correct" solution.

4.6.2 Non-Spherically Symmetric Swarms

At the roof, we now use the Robin condition for T (4.11) and the no-flux condition for ρ (4.13). The problem is no longer spherically symmetric, and thus we cannot measure numerical convergence rates by directly comparing the solutions to our previous results in Chapter 3. As such, we compare our numerical simulations to recorded observations. Note that unless otherwise specified, we use the parameters described in Table 2.1.

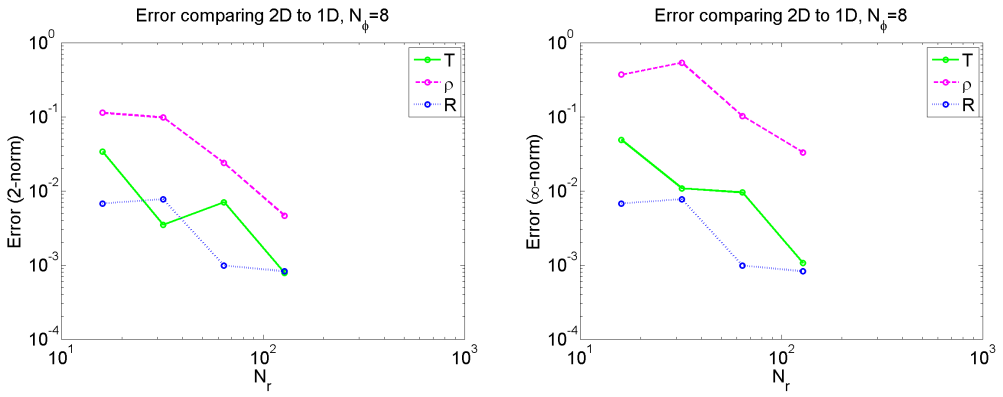

Figure 4.9: For a fixed M, we examine how increasing N affects the error in the ℓ^2-norm (left) and ℓ^∞-norm (right). The roof uses reflexive boundary conditions, while the exterior uses the Robin condition for u.

Comparison to Heinrich [14, Figure 1]

Following the contours reported by Heinrich [14, Figure 1], we took a swarm with 16,600 bees and exposed them an ambient temperature of 9°C; we simulated to steady state and compared our results with his observations. The results are depicted in Figures 4.10 and 4.11. Despite assuming the swarm-shape is hemispherical, our results have some quantitative and qualitative agreements with recorded observations.

In our numerical simulation, the maximum and minimum temperatures were respectively 33.6°C and 17.3°C, which is quite close to Heinrich's measured 35°C and 19°C. There was no density profile provided for us to compare against. However, as demonstrated in Figure 4.11, we observe the bees respond to the cold by forming a dense layer of bees around the exterior of the swarm. This behaviour agrees with the observations reported by Seeley [29].

However, the size of our swarm is quite different. Heinrich's contour measured 10 cm from the origin to the upper-right most point along the roof (which we call the *swarm width*), and 20 cm from the origin to the bottom along the interior (which we call the *swarm height*). Using *WebPlotDigitizer* [26] to extract the outermost contour of Heinrich's sketch and by assuming rotational symmetry, we calculated the volume as 6,603 cm^3 (this was calculated by a Riemann sum with cylindrical shells). However, our final radius was about 11.5 cm, which gives a volume of 3,185 cm^3 – thus the actual volume was more than double our simulated volume. This would mean our average density throughout the swarm is also incorrect.

This discrepancy was probably a result of the crude semicircle assumption, and perhaps also because our density profiles might not be correct (since density profiles determine the radius). Moreover, it is not surprising that our swarm height was not predicted correctly because the effects of gravity is not accounted for in our model, which would vertically stretch the swarm and increase the volume. Also, aside from modelling the roof's heat

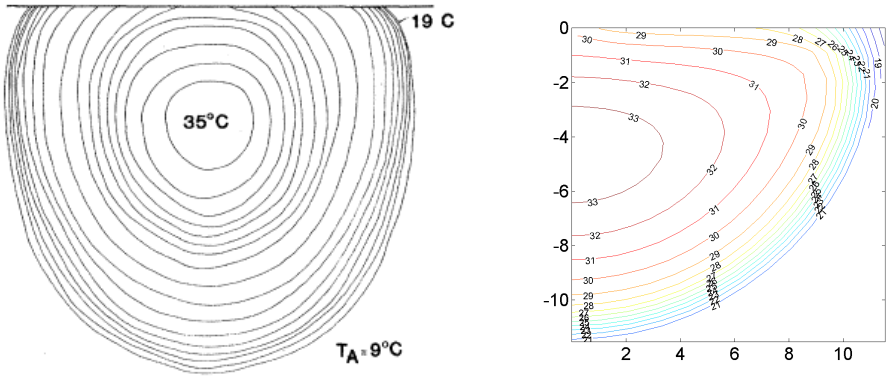

Figure 4.10: Biological experiments of Heinrich [14] (left) taken directly (but cropped) from [14, Figure 1] with permission; placed adjacent to our simulated solution. The swarm contained 16,600 bees and was exposed to an ambient temperature of 9°C.

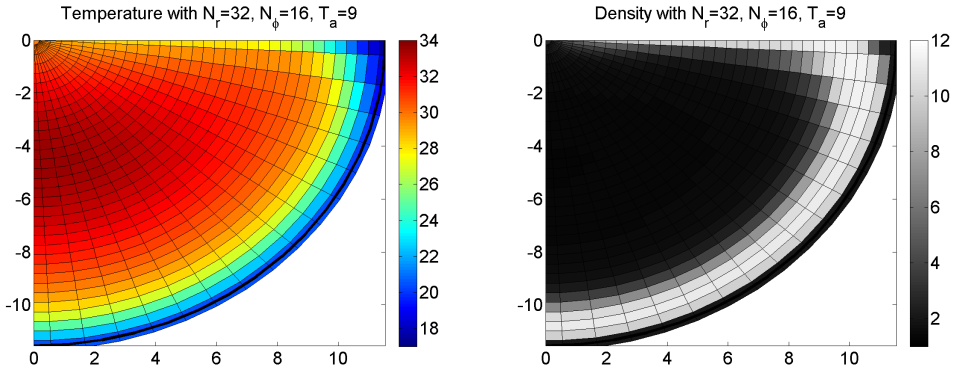

Figure 4.11: Another visualization of our simulated results from Figure 4.10, which is taken from [14, Figure 1]. The temperature profile (left) is placed adjacent to density profile (right). The swarm contained 16,600 bees and was exposed to an ambient temperature of 9°C.

transfer coefficient, the cylindrical Plexiglas that Heinrich used to capture the swarm was not accounted for in our model (which had a height of 43 cm and inner diameter of 29 cm [15]); the cylindrical vessel might have affected the swarm-shape. On the other hand, our predicted swarm width and contact area with the roof is reasonable – along the roof, Heinrich's reported 10 cm is similar to our simulated 11.5 cm.

Comparison to Heinrich [15, Figure 1]

We repeat our simulations for a smaller swarm described by Heinrich [15, Figure 1]. To match his experiment, we use 5,284 bees and a 5°C ambient temperature. As seen in Figures 4.12 and 4.13, our interior temperature is quantitatively similar to the recorded data. Heinrich's contour had a swarm width of about 5.8 cm and a swarm height of about

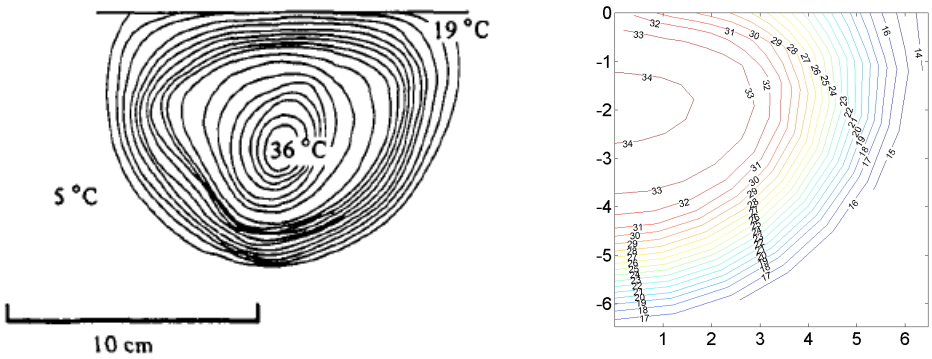

Figure 4.12: Biological experiments of Heinrich (left) taken directly (but cropped) from [15, Figure 1] with permission; placed adjacent to our simulated solution (right). The swarm contained 5,284 bees and was exposed to an ambient temperature of 5°C.

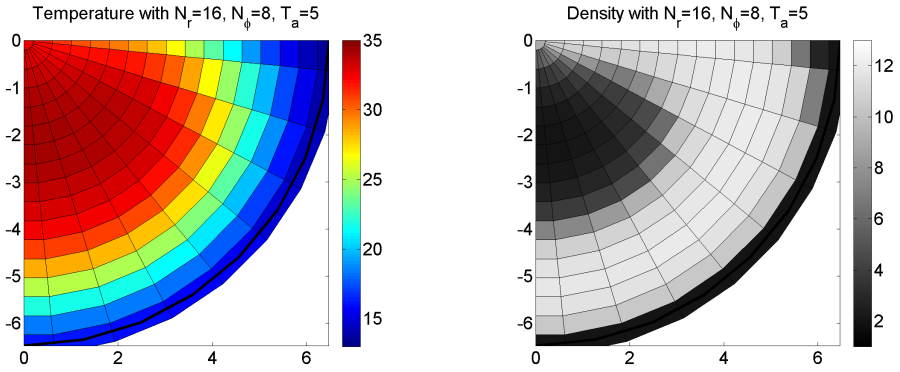

Figure 4.13: Another visualization of our simulated results from Figure 4.12, which is taken from [15, Figure 1]. The temperature profile (left) is placed adjacent to density profile (right). The swarm contained 5,284 bees and was exposed to an ambient temperature of 5°C.

10 cm. Our simulation had a hemispherical radius of about 6.5 cm. Once again, although we do not have the same volume or height, our computed swarm width (and thus also swarm contact area with roof) is reasonably similar to Heinrich's.

As seen in Figure 4.13, the smaller swarm appear to form a much thicker layer of insulating bees than in the larger swarm (Figure 4.11). Though this might seem to be a result of the colder ambient temperature (5°C vs 9°C), it is actually an artifact of the scale of the problem and the swarm size. Both thicknesses of the insulating swarm is roughly 2 cm, so in an absolute sense, they have the same thickness. However, the smaller swarm appears to form a thicker layer because their total radius is much smaller, so relative to the swarm size, the thickness of the insulating bees is thicker than in the larger swarm. Thus regardless of swarm size, a critical thickness of bees is required to trap heat in the inside.

Chapter 5

Conclusions and Future Work

5.1 Conclusions

We recreated and updated the numerical scheme to solve Watmough-Camazine's [40] model. In particular, we derived a new equation for swarm radius, along with a corresponding numerical method, which eliminated the need to rescale the density profile at every step. We then extended their model by relaxing the assumption of spherical symmetry; this was done by studying hemispherical swarms. In addition to the need to model the interaction between honeybees with the roof, an updated numerical scheme was developed to solve the equations in a two-dimensional computational domain. We produced results that at least qualitatively agree with experimental data.

5.2 General Swarm Shapes

In Chapter 4, we relaxed the assumption of spherical symmetry by assuming the swarm is a hemisphere. Naturally, the next step would be to allow shapes even more general than this. In doing so, the "swarm radius" $R(t)$ would need to be generalized to describe the shape of the swarm. One way would be to set $R = R(t, \phi)$, so that for each given ϕ, R would describe the distance between the origin and the swarm exterior. In doing so, our previous methods of introducing the independent variable becomes

$$x = \frac{r}{R(t, \phi)}, \tag{5.1}$$

which would now have ϕ dependence, and thus would create many computational issues. For instance, as demonstrated in Appendix C.1, this would lead to cross-derivative terms appearing in the Laplacian, and thus the numerical scheme would need to be updated to handle more terms. Moreover, the boundary conditions become more difficult to handle because the outward normals at the swarm exterior would no longer be trivial to compute.

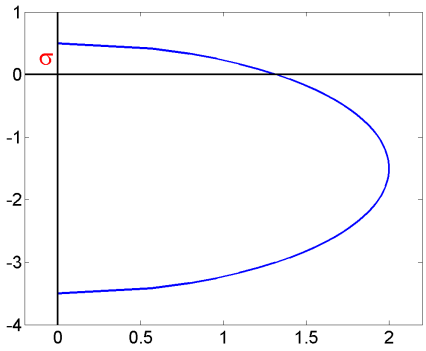

Figure 5.1: A visualization of the σ-shifted sphere. Everything above the roof would be truncated from the swarm.

Once the numerics have been updated, we may begin to explore swarm-shapes beyond spheres and hemispheres. As a first step, we could generalize the hemisphere by shifting a perfect sphere by σ and truncating it above the roof, as seen in Figure 5.1. Alternatively, we could take swarm sketches displayed in [11, 14, 15, 25] and impose a boundary; these results could be compared to their temperature isotherms. Afterwards, we can explore the important question, *what shape should a swarm take?*

5.3 Social Force

To study this, we could generalize our model by introducing a social force that describes how bees move throughout the entire computational domain. These equations would be similar to the work of Topaz et al. [39], where insect velocity is described by an integro-differential equation. Unlike our current model, this formulation would allow densities to go to zero. Thus determining the swarm's shape would be equivalent to tracking the interface where densities become zero, which could be done using level set methods. In addition to solving the swarm-shape problem, this approach would improve model flexibility (as effects such as gravity or heat convection could be incorporated into the social force), at the trade-off of computation sophistication. Although similar systems have been studied, such as in locust group movement [39], this approach has not been directly applied to honeybee thermoregulation, and thus the analysis and numerical schemes would need to be derived anew.

5.4 Bee-Balling

A fascinating extension of our swarming thermoregulation model is a parallel study of the *bee-balling* phenomenon [2]. Japanese honeybees have evolved a strange defence mechanism against predatory wasps where intruders are killed not by bites or stings, but rather by

Figure 5.2: Honeybee thermal defence, retrieved from `https://commons.wikimedia.org/wiki/File:Honeybee_thermal_defence01.jpg`. Used under Creative Commons Attribution-Share Alike 2.1 Japan license [38]. Two hornets engulfed and being heated by a ball of bees.

'baking'. Hundreds of honeybees swarm the intruder and collectively raise the temperature to a level that is tolerable to the bees but lethal for the wasp. Here, the bees exhibit an ability to much more rapidly change temperature and maintain levels within even tighter limits, but this is thermoregulation nonetheless. As such, our model could be extended to study bee-balling by determining appropriate modifications to our metabolism function and movement assumptions. Our resulting simulations can be compared to experimental data reported by Ken et al [19], and will shed insight how hundreds of bees can coordinate movement to exhibit such amazing control of their collective temperature.

Bibliography

[1] *Melbourne swarm*. https://commons.wikimedia.org/wiki/File:MelbourneSwarm.JPG, 2013. Accessed: November, 2015.

[2] D. P. Abrol, *Defensive behaviour of* apis cerana f. *against predatory wasps*, Journal of Apicultural Science, 50 (2006), pp. 39–46.

[3] W. R. Ashby, *Principles of the self-organizing system*, in Facets of Systems Science, vol. 7 of International Federation for Systems Research International Series on Systems Science and Engineering, Springer US, 1991, pp. 521–536.

[4] T. Basak, K. K. Rao, and A. Bejan, *A model for heat transfer in a honey bee swarm*, Chemical Engineering Science, 51 (1996), pp. 387–400.

[5] G. Collins, *Swarm of honey bees attached to a branch*. https://commons.wikimedia.org/wiki/File:Swarm_of_Honey_Bees_attached_to_a_branch.JPG, 2013. Accessed: November, 2015.

[6] S. M. Cully and T. D. Seeley, *Self-assemblage formation in a social insect: the protective curtain of a honeybee swarm*, Insectes Sociaux, 51 (2004), pp. 317–324.

[7] Engineering ToolBox, *Thermal Conductivity of some common Materials and Gases*. http://www.engineeringtoolbox.com/thermal-conductivity-d_429.html. Accessed: August, 2015.

[8] E. K. Eskov and V. A. Toboev, *Mathematical modeling of the temperature field distribution in insect winter clusters*, Biophysics, 54 (2009), pp. 85–89. Translated from *Biofizika* 54(1):114-119, 2009 (Russian).

[9] B. Feltz, M. Crommelinck, and P. Goujon, *Self-Organization and Emergence in Life Sciences*, Springer, 1 ed., 2006.

[10] R. C. Fetecau and A. Guo, *A mathematical model for flight guidance in honeybee swarms*, Bulletin of Mathematical Biology, (2012).

[11] J. B. Free, *The Social Organization of Honeybees*, Edward Arnold (Publishers) Limited, 1977.

[12] J. F. Harrison, J. H. Fewell, S. P. Roberts, and H. G. Hall, *Achievement of thermal stability by varying metabolic heat production in flying honeybees*, Science, 274 (1996), pp. 88–90.

[13] T. W. Hegarty, *Temperature coefficient Q_{10}, seed germination and other biological processes*, Nature, 243 (1985), pp. 305–306.

[14] B. Heinrich, *Energetics of honeybee swarm thermoregulation*, Science, 212 (1981), pp. 565–566.

[15] ——, *The mechanisms and energetics of honeybee swarm temperature regulation*, Journal of Experimental Biology, 91 (1981), pp. 25–55.

[16] B. Heinrich and H. Esch, *Thermoregulation in bees*, American Scientist, 82 (1994), pp. 164–170.

[17] J. C. Jones and B. P. Oldroyd, *Nest thermoregulation in social insects*, in Advances In Insect Physiology, S. J. Simpson, ed., vol. 33, Academic Press, 2007, pp. 153–191.

[18] A. Kammer and B. Heinrich, *Metabolic rates related to muscle activity in bumblebees*, Journal of Experimental Biology, 61 (1974), pp. 219–227.

[19] T. Ken, H. R. Hepburn, S. E. Radloff, Y. Yusheng, L. Yiqiu, Z. Danyin, and P. Neumann, *Heat-balling wasps by honeybees*, Naturwissenschaften, 92 (2005), pp. 492–495.

[20] M. Lemke and I. Lamprecht, *A model for heat production and thermoregulation in winter clusters of honey bees using differential heat conduction equations*, Journal of Theoretical Biology, 142 (1990), pp. 261–273.

[21] C.-C. Lin and L. Segel, *Mathematics Applied to Deterministic Problems in the Natural Sciences*, Society for Industrial and Applied Mathematics, Philadelphia, PA, 1988.

[22] M. R. Myerscough, *A simple model for temperature regulation in honeybee swarms*, Journal of Theoretical Biology, 162 (1993), pp. 381–393.

[23] S. A. Ocko and L. Mahadevan, *Collective thermoregulation in bee clusters*, Journal of the Royal Society Interface, 11 (2014), p. 20131033.

[24] S. W. Omholt and K. Lønvik, *Heat production in the winter cluster of the honeybee, apis mellifera. a theoretical study*, Journal of Theoretical Biology, 120 (1986), pp. 447 – 456.

[25] C. D. Owens, *The thermology of wintering honey bee colonies*, Technical Bulletin 1424, US Department of Agriculture, 1971. Downloaded from `http://www.beesource.com/resources/usda/the-thermology-of-wintering-honey-bee-colonies/`.

[26] A. Rohatgi, *WebPlotDigitizer*. `http://arohatgi.info/WebPlotDigitizer`. Accessed: May, 2015.

[27] T. M. Schaerf, J. C. Makinson, M. R. Myerscough, and M. Beekman, *Do small swarms have an advantage when house hunting? The effect of swarm size on nest-site selection by* Apis mellifera, Journal of the Royal Society Interface, 10 (2013), p. 20130533.

[28] T. Seeley and B. Heinrich, *Insect thermoregulation*, Wiley Press, New York, 1981, ch. Regulation of temperature in the nests of social insects, pp. 160–234.

[29] T. D. Seeley, *Honeybee Ecology*, Princeton University Press, 1985.

[30] ——, *Honeybee Democracy*, Princeton University Press, 2010.

[31] T. D. Seeley, R. A. Morse, and P. K. Visscher, *The natural history of the flight of honey bee swarms*, Psyche, 86 (1979), pp. 103–113.

[32] E. Southwick, *The honey bee cluster as a homeothermic superorganism*, Comparative Biochemistry and Physiology, 75A (1983), pp. 641–645.

[33] ——, *Bee hair structure and the effect of hair on metabolism at low temperature*, Journal of Apicultural Research, 24 (1985), pp. 144–149.

[34] E. E. Southwick and G. Heldmaier, *Temperature control in honey bee colonies*, BioScience, 37 (1987), pp. 395–399.

[35] A. Stabentheiner, H. Pressl, T. Papst, N. Hrassnigg, and K. Crailsheim, *Endothermic heat production in honeybee winter clusters*, Journal of Experimental Biology, 206 (2003), pp. 353–358.

[36] J. Strikwerda, *Finite Difference Schemes and Partial Differential Equations*, Society for Industrial and Applied Mathematics, 2nd ed., 2004.

[37] D. J. T. Sumpter and D. S. Broomhead, *Shape and dynamics of thermoregulating honey bee clusters*, Journal of Theoretical Biology, 204 (2000), pp. 1–14.

[38] Takahashi, *Honeybee thermal defence*. `https://commons.wikimedia.org/wiki/File:Honeybee_thermal_defence01.jpg`, 2005. Accessed: November, 2015.

[39] C. M. Topaz, M. R. D'Orsogna, L. Edelstein-Keshet, and A. J. Bernoff, *Locust dynamics: Behavioral phase change and swarming*, PLoS Computational Biology, 8 (2012), p. e1002642.

[40] J. Watmough and S. Camazine, *Self-organized thermoregulation of honeybee clusters*, Journal of Theoretical Biology, 176 (1995), pp. 391–402.

[41] M. Winston, *Swarming, afterswarming, and reproductive rate of unmanaged honeybee colonies (apis mellifera)*, Insectes Sociaux, 27 (1980), pp. 391–398.

[42] M.-X. Yang, Z.-W. Wang, H. Li, Z.-Y. Zhang, K. Tan, S. E. Radloff, and H. R. Hepburn, *Thermoregulation in mixed-species colonies of honeybees (apis cerana and apis mellifera)*, Journal of Insect Physiology, 56 (2010), pp. 706 – 709.

Appendix A

Derivation of Equations in 1D

A.1 Deriving the Differential Equation for Swarm Radius

We show in detail the derivation of Equation (2.6) from Equation (2.5). Recall Equation (2.5)

$$4\pi \int_0^{R(t)} r^2 \rho(t,r) \mathrm{d}r = B_0.$$

Taking the time derivative of both sides gives

$$\frac{\mathrm{d}}{\mathrm{d}t} \int_0^{R(t)} r^2 \rho(t,r) \mathrm{d}r = 0.$$

By applying Leibniz's rule for differentiation under the integral sign, we obtain

$$\int_0^{R(t)} r^2 \frac{\partial}{\partial t} \rho(t,r) \mathrm{d}r + R(t)^2 \rho(R(t),t) R'(t) = 0.$$

Applying Equation (2.3) in spherical coordinates and the fundamental theorem of calculus gives

$$\left(r^2 \mu(\rho) \frac{\partial \rho}{\partial r} - r^2 \chi(T) \rho \frac{\partial T}{\partial r} \right) \Bigg|_0^{R(t)} = -R(t)^2 \rho(R(t),t) R'(t).$$

Evaluating and rearranging gives us the desired differential equation for $R(t)$

$$\frac{\mathrm{d}R}{\mathrm{d}t} = \left(-\frac{\mu}{\rho} \frac{\partial \rho}{\partial r} + \chi \frac{\partial T}{\partial r} \right) \Bigg|_{r=R(t)}.$$

A.2 Transforming Partial Differential Equations to Mapped Coordinates

In this section, we demonstrate that Equation (2.2)

$$\frac{\partial T}{\partial t} = \frac{1}{r^2}\frac{\partial}{\partial r}\left[r^2\lambda(\rho)\frac{\partial T}{\partial r}\right] + \rho f(T)$$

becomes Equation (3.4)

$$c\frac{\partial u}{\partial t} - \frac{cxR'}{R}\frac{\partial u}{\partial x} = \frac{1}{x^2R^2}\frac{\partial}{\partial x}\left[x^2\lambda\frac{\partial u}{\partial x}\right] + vf$$

with the change of variables $x = \frac{r}{R(t)}$ and

$$u(t,x) = T(t, r(t,x)).$$

We'll begin with the derivation of the left-hand side. Consider $\frac{\mathrm{d}}{\mathrm{d}t}[T(t,r(t,x))]$, which from the chain rule is

$$\frac{\mathrm{d}}{\mathrm{d}t}[T(t,r(t,x))] = \underbrace{\frac{\partial}{\partial t}[T(t,r)]}_{(*_1)}\frac{\partial t}{\partial t} + \underbrace{\frac{\partial}{\partial r}[T(t,r)]\frac{\partial r}{\partial t}}_{(*_2)}.$$

The term $(*_1)$ is exactly the time derivative term in Equation (2.2) that we wish to solve for. In $(*_2)$, since $r = xR(t)$, it follows that $\frac{\partial r}{\partial t} = xR'(t)$, and a second application of the chain rule yields

$$\frac{\partial}{\partial x}[T(t,r(t,x))] = \frac{\partial}{\partial r}[T(t,r)]\underbrace{\frac{\partial r}{\partial x}}_{=R(t)} + \frac{\partial}{\partial r}[T(t,r)]\underbrace{\frac{\partial t}{\partial x}}_{=0}$$

$$\implies \qquad \frac{\partial}{\partial r}[T(t,r)] = \frac{\partial}{\partial x}[T(r(t,x),t)]\frac{1}{R(t)}.$$

Note $\frac{\partial}{\partial t}[T(t,r(t,x))] = \frac{\partial u}{\partial t}$. Thus solving for $(*_1)$ gives

$$\frac{\partial}{\partial t}[T(t,r)] = \frac{\partial}{\partial x}[T(r(t,x),t)] - \frac{xR'(t)}{R(t)}\frac{\partial}{\partial x}[T(r(t,x),t)].$$

Hence, the left-hand side of Equation (2.2) becomes

$$c\frac{\partial u}{\partial t} - c\frac{xR'(t)}{R(t)}\frac{\partial u}{\partial x},$$

as required.

As for the right-hand side, since $\frac{\partial t}{\partial x} = 0$ and $\frac{\partial r}{\partial x} = R(t)$, we have

$$\frac{\partial}{\partial r} \equiv R(t)\frac{\partial}{\partial x},$$

which then gives

$$\begin{aligned}\frac{1}{r^2}\frac{\partial}{\partial r}\left[r^2\lambda\frac{\partial T}{\partial r}\right] &= \frac{1}{(xR(t))^2}\cdot\frac{1}{R(t)}\frac{\partial}{\partial x}\left[(xR(t))^2\lambda\frac{1}{R(t)}\frac{\partial u}{\partial x}\right] \\ &= \frac{1}{x^2R(t)^2}\frac{\partial}{\partial x}\left[x^2\lambda\frac{\partial u}{\partial x}\right];\end{aligned}$$

and finally

$$\rho f = vf.$$

Thus putting the left- and right-hand sides together, we obtain Equation (3.4)

$$c\frac{\partial u}{\partial t} - \frac{cxR'}{R}\frac{\partial u}{\partial x} = \frac{1}{x^2R^2}\frac{\partial}{\partial x}\left[x^2\lambda\frac{\partial u}{\partial x}\right] + vf.$$

For density, the transformation from Equation (2.4) to Equation (3.5) follows a similar argument.

A.3 Transforming Swarm Radius Equations to Mapped Coordinates

We show the derivation of Equation (3.6) from Equation (2.5), which is

$$4\pi\int_0^{R(t)} r^2\rho(t,r)\mathrm{d}r = B_0.$$

Fix t and use integration by substitution to transform from r to x. Denote $f(r) = r^2\rho(r)$, and change the limits of integration from $[0, R]$ to $[0, 1]$, so with $\phi(x) = xR$ we obtain

$$\begin{aligned}\int_0^R f(r)\mathrm{d}r &= \int_0^1 f(\phi(x))\phi'(x)\mathrm{d}x \\ &= \int_0^1 x^2R(t)^2\rho(xR)R(t)\mathrm{d}x.\end{aligned}$$

Because $xR = r$ and $\rho(r) = v(x)$, the normalized Equation (2.5) becomes

$$4\pi\int_0^1 x^2R(t)^3v(t,x)\mathrm{d}x = B_0.$$

Appendix B

Derivations of Equations for Hemispherical Swarms

B.1 Outward Normal at Roof

Note all $\mathbb{R}^3$ vectors in this subsection correspond respectively to (x, y, z). That is,

$$\vec{v} = (v_1, v_2, v_3) = v_1\vec{e}_x + v_2\vec{e}_y + v_3\vec{e}_z.$$

Clearly, the unit outward normal at the roof is

$$\vec{n} = (0, 0, 1) = \vec{e}_z. \tag{B.1}$$

We need to express this in spherical coordinates. Recall in spherical coordinates, the unit vectors are

$$\vec{e}_r = (\cos\theta\sin\phi, \sin\theta\sin\phi, \cos\phi), \tag{B.2}$$
$$\vec{e}_\theta = (-\sin\theta, \cos\theta, 0), \tag{B.3}$$
$$\vec{e}_\phi = (\cos\theta\cos\phi, \sin\theta\cos\phi, -\sin\phi). \tag{B.4}$$

At the roof, we have $\theta = 0$, $\phi = \frac{\pi}{2}$, and $r \in [0, R(t)]$. Notice that

$$\vec{e}_\phi = (0, 0, -1) = -\vec{e}_z. \tag{B.5}$$

Thus

$$\vec{n} = -\vec{e}_\phi. \tag{B.6}$$

Hence, with $\nabla T = \frac{\partial T}{\partial r}\vec{e}_r + \frac{1}{r}\frac{\partial T}{\partial \phi}\vec{e}_\phi$, we have

$$\nabla T \cdot \vec{n} = -\frac{1}{r}\frac{\partial T}{\partial \phi}. \tag{B.7}$$

B.2 Discretization at Origin in Hemisphere

Here, we derive a spatial discretization for T at the origin (which features a coordinate singularity) for a hemispherical domain in spherical coordinates. We follow work similar to Strikwerda [36, Chapter 12.6], which describes a finite difference scheme for Poisson's equation in polar coordinates.

Fixing t, from Equation (4.1) we have Poisson's equation

$$F = \frac{1}{r^2}\frac{\partial}{\partial r}\left[r^2\lambda\frac{\partial T}{\partial r}\right] + \frac{1}{r\sin\phi}\frac{\partial}{\partial\phi}\left[\frac{\lambda\sin\phi}{r}\frac{\partial T}{\partial\phi}\right], \tag{B.8}$$

where

$$F(r) = c\frac{\partial T}{\partial t} - \rho f. \tag{B.9}$$

To derive an equation, we integrate equation (B.8) over a sphere centred at the origin with radius ε, which gives (with θ symmetry)

$$\begin{aligned}\underbrace{2\pi\int_0^{\pi}\int_0^{\varepsilon} Fr^2\sin\phi\,\mathrm{d}r\mathrm{d}\phi}_{(*_0)} = &\underbrace{2\pi\int_0^{\pi}\int_0^{\varepsilon}\sin\phi\frac{\partial}{\partial r}\left[r^2\lambda\frac{\partial T}{\partial r}\right]\mathrm{d}r\mathrm{d}\phi}_{(*_1)}\\ &+\underbrace{2\pi\int_0^{\pi}\int_0^{\varepsilon} r\frac{\partial}{\partial\phi}\left[\frac{\lambda\sin\phi}{r}\frac{\partial T}{\partial\phi}\right]\mathrm{d}r\mathrm{d}\phi}_{(*_2)}\end{aligned} \tag{B.10}$$

We now note that everything in the region $\phi \in (0, \frac{\pi}{2})$ is ignored as it is not in the computational domain, and thus assume everything is zero in this region. Hence we switch ϕ's limits of integration to be from $\frac{\pi}{2}$ to π.

Firstly, consider $(*_0)$. Since ε is small, we can approximate F in the integral using the Taylor series

$$F(\xi) = F(0) + O(\Delta r)$$

and dropping the $O(\Delta r)$ terms. Thus

$$\begin{aligned}(*_0) &= 2\pi F(0)\int_{\frac{\pi}{2}}^{\pi}\int_0^{\varepsilon} r^2\sin\phi\,\mathrm{d}r\mathrm{d}\phi\\ &= 2\pi F(0)\int_{\frac{\pi}{2}}^{\pi}\frac{r^3}{3}\Big|_0^{\varepsilon}\sin\phi\,\mathrm{d}\phi\\ &= 2\pi F(0)\frac{(\frac{\Delta r}{2})^3}{3}(-\cos\phi)\Big|_{\frac{\pi}{2}}^{\pi}\\ &= \frac{\pi}{12}F(0)\Delta r^3.\end{aligned}$$

For $(*_1)$, by applying the fundamental theorem of calculus we obtain

$$(*_1) = 2\pi \int_{\frac{\pi}{2}}^{\pi} \sin\phi \varepsilon^2 \left(\lambda \frac{\partial T}{\partial r}\right)\Big|_{r=\varepsilon} \mathrm{d}\phi$$

Note $T_{0,0} = T_{0,1} = T_{0,2} = \cdots = T_{0,M}$, so we refer to the this as T_0. Notice a centred difference scheme at $r = \frac{\Delta r}{2}$ gives an equation involving T_0, hence we choose $\varepsilon = \frac{\Delta r}{2}$ (note since we are in a semicircle, R does not depend on ϕ, and hence ε has no ϕ-dependence). Discretizing the derivative with centre-differencing and the integral with a right-side Riemann sum gives

$$\begin{aligned}(*_1) &= 2\pi \int_{\frac{\pi}{2}}^{\pi} \sin\phi \left(\frac{\Delta r}{2}\right)^2 \lambda_{\frac{1}{2},j} \frac{T_{1,j} - T_0}{\Delta r} \mathrm{d}\phi \\ &= \frac{\pi}{2} \sum_{j=1}^{M} \sin\phi_j \lambda_{\frac{1}{2},j} \Delta r (T_{1,j} - T_0) \Delta\phi,\end{aligned}$$

where $\Delta\phi = \frac{\frac{\pi}{2}}{M}$.

For $(*_2)$, switching the order of integration and applying the fundamental theorem of calculus gives

$$\begin{aligned}(*_2) &= 2\pi \int_{0}^{\varepsilon} r \left(\frac{\lambda \sin\phi}{r} \frac{\partial T}{\partial \phi}\right)\Big|_{\frac{\pi}{2}}^{\pi} \mathrm{d}r \\ &= -2\pi \int_{0}^{\varepsilon} \lambda \frac{\partial T}{\partial \phi}\Big|_{\frac{\pi}{2}} \mathrm{d}r.\end{aligned}$$

If we use the reflexive boundary condition (4.50), then $\frac{\partial T}{\partial \phi}$ is zero at $\phi = \frac{\pi}{2}$ and thus $(*_2)$ is zero. However, if we use the Robin boundary condition for T (4.11), $\frac{\partial T}{\partial \phi}$ is non-zero and must be handled separately. Denote the integrand by

$$G(r) = \lambda \frac{\partial T}{\partial \phi}\Big|_{\phi=\frac{\pi}{2}}.$$

Using the Robin boundary condition (4.11), we have

$$G(r) = -r(T_a - T). \tag{B.11}$$

Since ε is small, we can approximate the integrand with a Taylor series

$$G(\xi) = G(0) + O(\Delta r)$$

and dropping the $O(\Delta r)$ terms. Hence

$$\begin{aligned}(*_2) &= -2\pi \int_0^{\varepsilon} G(r)\mathrm{d}r \\ &\approx -2\pi G(0) \int_0^{\varepsilon} \mathrm{d}r \\ &= 0,\end{aligned}$$

since $G(0) = 0$.

So we currently have

$$\frac{\pi}{12}F(0)\Delta r^3 = \frac{\pi}{2}\Delta r \Delta\phi \sum_{j=1}^{M} \sin\phi_j \lambda_{\frac{1}{2},j}(T_{1,j} - T_0),$$

which is equivalent to

$$F(0) = \frac{6\Delta\phi}{\Delta r^2} \sum_{j=1}^{M} \sin\phi_j \lambda_{\frac{1}{2},j}(T_{1,j} - T_0). \tag{B.12}$$

Solving for T_0 gives

$$T_0 = \frac{6\Delta\phi}{\Delta r^2 \beta} \sum_{j=1}^{M} \sin\phi_j \lambda_{\frac{1}{2},j} T_{1,j} - \frac{1}{\beta}F(0), \tag{B.13}$$

where $\beta = \frac{6\Delta\phi}{\Delta r^2} \sum_{j=1}^{M} \sin\phi_j \lambda_{\frac{1}{2},j}$.

It is interesting to note upon making the correct assumptions, our two-dimensional and one-dimensional discretizations of the origins are equivalent. By assuming that T and λ has no ϕ dependence, upon taking $M \to \infty$, the right-hand side of Equation (B.12) becomes

$$\begin{aligned}\frac{6\Delta\phi}{\Delta r^2} \sum_{j=1}^{M} \sin\phi_j \lambda_{\frac{1}{2}}(T_1 - T_0) &= \frac{6}{\Delta r^2}\lambda_{\frac{1}{2}}(T_1 - T_0) \int_{\frac{\pi}{2}}^{\pi} \sin(\phi)\mathrm{d}\phi \\ &= 6\lambda_{\frac{1}{2}} \frac{T_1 - T_0}{\Delta r^2},\end{aligned}$$

which upon transformation from r to x is equivalent to the one-dimensional discretization of the origin (Equation (3.24)).

Appendix C

Generalized Two-Dimensional Swarms

C.1 Transforming Equations to Mapped Coordinates in 2D

In this section, we transform Equations (2.1) and (2.3) into a mapped coordinate system (defined below) for a convex two-dimensional domain that is not necessarily a semicircle, such as the one presented in Figure C.1. Suppose for every fixed time t and every fixed $\phi \in [\frac{\pi}{2}, \pi]$, the swarm exterior is distance $R(t, \phi)$ from the origin. Hence $R(t, \phi)$ describes the shape of the swarm at every time. We introduce the coordinate transformation

$$x = \frac{r}{R(t, \phi)} \tag{C.1}$$

and corresponding dependent variables

$$u(t, x, \phi) = T(t, r(x, \phi, t), \phi), \tag{C.2}$$
$$v(t, x, \phi) = \rho(t, r(x, \phi, t), \phi). \tag{C.3}$$

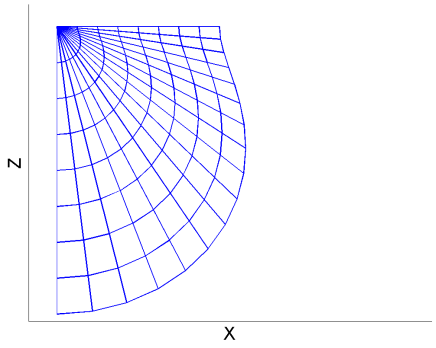

Figure C.1: In the future, we may consider two-dimensional computational domains that are more general than semicircles.

We also introduce the notation

$$\dot{R}(t,\phi) = \frac{\partial R}{\partial t}, \tag{C.4}$$

$$P(t,\phi) = \frac{\partial R}{\partial \phi}. \tag{C.5}$$

Now, recall if we have $g(t,r,\phi)$ and its corresponding function $\tilde{g}(t,x,\phi)$, then the change of partials can be expressed conveniently as the matrix-vector multiplication

$$\begin{bmatrix} g_t \\ g_r \\ g_\phi \end{bmatrix} = \begin{bmatrix} t_t & x_t & \phi_t \\ t_r & x_r & \phi_r \\ t_\phi & x_\phi & \phi_\phi \end{bmatrix} \begin{bmatrix} \tilde{g}_t \\ \tilde{g}_x \\ \tilde{g}_\phi \end{bmatrix}. \tag{C.6}$$

Evaluating the partials gives

$$\begin{bmatrix} g_t \\ g_r \\ g_\phi \end{bmatrix} = \begin{bmatrix} 1 & -\frac{x\dot{R}}{R} & 0 \\ 0 & \frac{1}{R} & 0 \\ 0 & -\frac{xP}{R} & 1 \end{bmatrix} \begin{bmatrix} \tilde{g}_x \\ \tilde{g}_\phi \\ \tilde{g}_t \end{bmatrix}. \tag{C.7}$$

That is,

$$\frac{\partial}{\partial t} \equiv -\frac{x\dot{R}}{R}\frac{\partial}{\partial x} + \frac{\partial}{\partial t}, \tag{C.8}$$

$$\frac{\partial}{\partial r} \equiv \frac{1}{R}\frac{\partial}{\partial x} \tag{C.9}$$

$$\frac{\partial}{\partial \phi} \equiv -\frac{xP}{R}\frac{\partial}{\partial x} + \frac{\partial}{\partial \phi}. \tag{C.10}$$

Recall Equation (2.1)

$$c\frac{\partial T}{\partial t} = \nabla \cdot (\lambda \nabla T) + \rho f,$$

where $T = T(t,r,\phi)$. In spherical coordinates with symmetry about θ, this becomes

$$\underbrace{c\frac{\partial T}{\partial t}}_{(*_1)} = \underbrace{\frac{1}{r^2}\frac{\partial}{\partial r}\left[r^2\lambda\frac{\partial T}{\partial r}\right]}_{(*_2)} + \underbrace{\frac{1}{r\sin\phi}\frac{\partial}{\partial \phi}\left[\frac{\lambda\sin\phi}{r}\frac{\partial T}{\partial \phi}\right]}_{(*_3)} + \underbrace{\rho f}_{(*_4)}. \tag{C.11}$$

First, transform $(*_1)$. From Equation (C.8), we obtain

$$(*_1) = c\frac{\partial u}{\partial t} - c\frac{x\dot{R}}{R}\frac{\partial u}{\partial x}.$$

Next, with Equation (C.9) and the fact that $\frac{\partial R}{\partial x} = 0$, we get

$$(*_2) = \frac{1}{x^2R^2}\frac{\partial}{\partial x}\left[x^2\lambda\frac{\partial u}{\partial x}\right].$$

Applying Equation (C.10) twice gives

$$\begin{aligned}(*_3) =& \frac{1}{xR\sin\phi}\frac{\partial}{\partial\phi}\left[\frac{\lambda\sin\phi}{xR}\frac{\partial u}{\partial\phi} - \frac{\lambda\sin\phi P}{R^2}\frac{\partial u}{\partial x}\right] \\ &- \frac{P}{R^2\sin\phi}\frac{\partial}{\partial x}\left[\frac{\lambda\sin\phi}{xR}\frac{\partial u}{\partial\phi} - \frac{\lambda\sin\phi P}{R^2}\frac{\partial u}{\partial x}\right]\end{aligned}$$

Finally,

$$(*_4) = vf.$$

Thus in spherical coordinates, our partial differential equation becomes

$$\begin{aligned}c\frac{\partial u}{\partial t} - c\frac{x\dot{R}}{R}\frac{\partial u}{\partial x} =& vf + \frac{1}{x^2R^2}\frac{\partial}{\partial x}\left[x^2\lambda\frac{\partial u}{\partial x}\right] \\ &+ \frac{1}{xR\sin\phi}\frac{\partial}{\partial\phi}\left[\frac{\lambda\sin\phi}{xR}\frac{\partial u}{\partial\phi} - \frac{\lambda\sin\phi P}{R^2}\frac{\partial u}{\partial x}\right] \\ &- \frac{P}{R^2\sin\phi}\frac{\partial}{\partial x}\left[\frac{\lambda\sin\phi}{xR}\frac{\partial u}{\partial\phi} - \frac{\lambda\sin\phi P}{R^2}\frac{\partial u}{\partial x}\right].\end{aligned} \tag{C.12}$$

Similarly, from Equation (2.3)

$$\frac{\partial\rho}{\partial t} = \nabla\cdot(\mu\nabla\rho) - \nabla\cdot(\chi\rho\nabla T),$$

we obtain the new equation

$$\begin{aligned}\frac{\partial v}{\partial t} - \frac{x\dot{R}}{R}\frac{\partial v}{\partial x} =& \frac{1}{x^2R^2}\frac{\partial}{\partial x}\left[x^2\mu\frac{\partial v}{\partial x} - x^2\chi v\frac{\partial u}{\partial x}\right] \\ &+ \frac{1}{xR\sin\phi}\frac{\partial}{\partial\phi}\left[\frac{\mu\sin\phi}{xR}\frac{\partial v}{\partial\phi} - \frac{\mu\sin\phi P}{R^2}\frac{\partial v}{\partial x}\right] \\ &- \frac{1}{xR\sin\phi}\frac{\partial}{\partial\phi}\left[\frac{\chi v\sin\phi}{xR}\frac{\partial u}{\partial\phi} - \frac{\chi v\sin\phi P}{R^2}\frac{\partial u}{\partial x}\right] \\ &- \frac{P}{R^2\sin\phi}\frac{\partial}{\partial x}\left[\frac{\mu\sin\phi}{xR}\frac{\partial v}{\partial\phi} - \frac{\mu\sin\phi P}{R^2}\frac{\partial v}{\partial x}\right] \\ &+ \frac{P}{R^2\sin\phi}\frac{\partial}{\partial x}\left[\frac{\chi v\sin\phi}{xR}\frac{\partial u}{\partial\phi} - \frac{\chi v\sin\phi P}{R^2}\frac{\partial u}{\partial x}\right].\end{aligned} \tag{C.13}$$

C.2 Resolving Coordinate Singularity at the Interior

Consider the terms involving ∂_ϕ in Equations (4.17, 4.18). Notice there is a coordinate singularity at $\phi = \pi$ due to the $\sin(\phi)$ in the denominator. To resolve this we use a similar technique to the one-dimensional coordinate singularity at $r = 0$.

Consider the $\frac{\partial}{\partial\phi}\frac{\partial}{\partial\phi}$ term in equation (4.17). Expanding with the product rule gives

$$\begin{aligned}\frac{1}{x^2R\sin\phi}\frac{\partial}{\partial\phi}\left[\sin\phi\frac{\lambda u_\phi}{R}\right]\Bigg|_{\phi=\pi} &= \frac{1}{x^2R\sin\phi}\left(\cos\phi\frac{\lambda u_\phi}{R}+\sin\phi\frac{\partial}{\partial\phi}\left[\frac{\lambda u_\phi}{R}\right]\right)\\ &= \frac{1}{x^2R}\left(\cos\phi\frac{\frac{\lambda u_\phi}{R}}{\sin\phi}+\frac{\partial}{\partial\phi}\left[\frac{\lambda u_\phi}{R}\right]\right).\end{aligned}$$

Since $u_\phi = 0$, a $\frac{0}{0}$ singularity is present, so L'Hôpital's rule, along with further simplifications, gives

$$\frac{1}{x^2R\sin\phi}\frac{\partial}{\partial\phi}\left[\sin\phi\frac{\lambda u_\phi}{R}\right]\Bigg|_{\phi=\pi} = \frac{2}{x^2R}\frac{\partial}{\partial\phi}\left[\frac{\lambda u_\phi}{R}\right]\Bigg|_{\phi=\pi}. \tag{C.14}$$

Next, consider the $\frac{\partial}{\partial\phi}\frac{\partial}{\partial x}$ term in equation (4.17). Although $u_x \neq 0$, we have $P = R_\phi = 0$ by the rotational symmetry. Hence, a similar derivation to above gives

$$\frac{1}{xR\sin\phi}\frac{\partial}{\partial\phi}\left[\frac{\lambda\sin\phi P}{R^2}\frac{\partial u}{\partial x}\right]\Bigg|_{\phi=\pi} = \frac{2}{xR}\frac{\partial}{\partial\phi}\left[\frac{\lambda P u_x}{R^2}\right]\Bigg|_{\phi=\pi} \tag{C.15}$$

C.3 Discretizing the Swarm Radius Integral

In this section, we discretize Equations (4.3) (4.19), the integral that counts the number of bees in the swarm. Note that here we assume $R = R(t,\phi)$, which is more general than a hemisphere.

Recall Equation (4.3)

$$2\pi\int_0^\pi\left(\int_0^{R(t,\phi)}\rho(r,\phi)r^2\mathrm{d}r\right)\sin(\phi)\mathrm{d}\phi = B_0. \tag{C.16}$$

So for a fixed ϕ_j,

$$\int_0^{R(t,\phi)}\rho(r,\phi)r^2\mathrm{d}r = \Delta r_j\sum_{i=0}^{N}c_i\rho_{i,j}r_{i,j}^2,$$

where c_i is the trapezoidal Riemann sum coefficient for r

$$c_i = \begin{cases}\frac{1}{2}, & \text{if } i = 0, N,\\ 1, & \text{if } i \neq 0, N.\end{cases}$$

Discretizing the integral in ϕ gives

$$B_0 = 2\pi\Delta\phi\sum_{j=0}^{M}\tilde{c}_j\sin(\phi_j)\Delta r_j\sum_{i=0}^{N}c_i\rho_{i,j}r_{i,j}^2, \tag{C.17}$$

where $\tilde{c}_j$ is the trapezoidal Riemann sum coefficient for ϕ

$$\tilde{c}_j = \begin{cases} \frac{1}{2}, & \text{if } j = 0, M, \\ 1, & \text{if } j \neq 0, M. \end{cases}$$

Finally, transforming to the dimensionless coordinate system gives

$$B_0 = 2\pi \Delta x \Delta \phi \sum_{j=0}^{M} \tilde{c}_j \sin(\phi_j) R_j^3 \sum_{i=0}^{N} c_i x_i^2 v_{i,j}. \tag{C.18}$$

Switching the sums yields the alternative equation

$$B_0 = 2\pi \Delta x \Delta \phi \sum_{i=0}^{N} c_i x_i^2 \sum_{j=0}^{M} \tilde{c}_j \sin(\phi_j) R_j^3 v_{i,j}. \tag{C.19}$$